Bacterial inhibition of Fas-mediated killing promotes neuroinvasion and persistence

Claire Maudet[1,*], Marouane Kheloufi[1,*], Sylvain Levallois[1], Julien Gaillard[1], Lei Huang[1], Charlotte Gaultier[1], Yu-Huan Tsai[1,‡], Olivier Disson[1], Marc Lecuit[1,2,3,†]

[1] Institut Pasteur, Université de Paris, Inserm U1117, Biology of Infection Unit, 75015 Paris, France

[2] Institut Pasteur, National Reference Center and WHO Collaborating Center Listeria, 75015 Paris, France

[3] Necker-Enfants Malades University Hospital, Division of Infectious Diseases and Tropical Medicine, APHP, Institut Imagine, 75006, Paris, France

* These authors share first authorship

† **Correspondence to:** marc.lecuit@pasteur.fr

‡ **Current address:** Institute of Microbiology and Immunology, National Yang-Ming University, Taipei, Taiwan

Abstract

Central nervous system infections are amongst the most severe[1,2], yet the mechanisms by which pathogens access the brain remain poorly understood. The model microorganism *Listeria monocytogenes* (*Lm*) is a major foodborne pathogen that causes neurolisteriosis, one of the deadliest central nervous system infections[3,4]. While immunosuppression is a well-established host risk factor for neurolisteriosis[3,5], little is known regarding the bacterial factors underlying *Lm* neuroinvasion. Here, we have developed a clinically-relevant experimental model of neurolisteriosis, using hypervirulent neuroinvasive strains[6] inoculated in a humanized mouse model of infection[7], and we show that the bacterial protein InlB protects infected monocytes from $CD8^+$ T-cells Fas-mediated cell death, in a c-Met/PI3-kinase/FLIP-dependent manner. This blockade of anti-*Lm* specific cellular immune killing lengthens infected monocytes lifespan, favoring *Lm* transfer from infected monocytes to the brain. The intracellular niche created by InlB-mediated cell-autonomous immune resistance also promotes *Lm* fecal shedding, accounting for InlB selection as a *Lm* core virulence gene. We have uncovered an unanticipated specific mechanism by which a bacterial pathogen confers to the cells it infects an increased lifespan by rendering them resistant to cell-mediated immunity. This promotes *Lm* within-host persistence and dissemination to the central nervous system, and transmission.

Listeria monocytogenes (*Lm*) factors promoting its neuroinvasion and their mechanisms of action are poorly understood. Earlier studies have pointed towards the involvement of monocytes in transferring *Lm* from the blood to the central nervous system (CNS)[8,9]. However, these investigations were performed with poorly neuroinvasive[6] reference laboratory *Lm* strains, which require very high bacterial inocula to induce CNS infection in experimental animal models. This is consistent with the observation that these strains belong to clonal complexes very rarely responsible for human neurolisteriosis[3,6]. In contrast, clinically-associated clonal complexes are hypervirulent and more neuroinvasive[6]. In order to investigate the mechanisms underlying *Lm* neuroinvasion, we developed a clinically-relevant experimental model of neurolisteriosis based on the inoculation of hypervirulent neuroinvasive *Lm* strains[6] in a humanized mouse model[7].

Monocytes mediate *Lm* neuroinvasion

We orally inoculated *Lm* in humanized KIE16P mice, which are permissive to orally-acquired listeriosis[7]. In contrast to the reference strain EGDe that belongs to the clonal complex (CC) 9[10,11], clinical isolates belonging to the hypervirulent clonal complexes CC1, 4 and 6 systematically induce high-level neuroinvasion, as previously reported[6], starting at 3 days post-inoculation (dpi) (Fig. 1a). At 5 dpi, the bacterial brain load is the same with or without administration of gentamicin (Fig. 1b, Extended Data Fig. 1a), an antibiotic that kills extracellular (Extended Fig. 1b) but not intracellular *Lm*[12], indicating that intracellular bacteria are involved in neuroinvasion. Consistently, neuroinvasive *Lm* are detected in the blood (Extended Data Fig. 1c), and are predominantly found in inflammatory monocytes ($CD45^+$ $CD11b^+Ly6C^+$ $CD3^-$ $CD19^-$ $CD11c^-$ $Ly6G^-$) in the blood and spleen (Fig. 1c, d, Extended Data Fig. 1d-e), suggesting that monocytes are involved in *Lm* neuroinvasion. This was confirmed by infecting *Ccr2*$^{-/-}$ mice, in which monocytes are retained in the bone marrow and are therefore less abundant in the blood and spleen[13] (Extended Data Fig. 1f). Indeed, from 1 to 3 dpi, more bacteria are gradually recovered from the brain of WT mice as compared to *Ccr2*$^{-/-}$ mice (Fig. 1e). Moreover, the transfer of infected monocytes from donor-infected mice into gentamicin-treated uninfected recipient mice (Extended Data Fig. 1g) is sufficient to induce neuroinvasion as early as day 2 post-transfer (Fig. 1f). In contrast, the transfer of infected monocytes from mice expressing the diphteria toxin (DT) receptor in myeloid cells (*LysM*-$CreER^{T2}$×iDTR) into recipient mice treated with DT to deplete transferred monocytes, leads to liver and spleen infection but no brain infection, even as late as 4 days post-transfer (Extended Data Fig. 1h, i). Together, these results indicate that infected monocytes are necessary and sufficient to induce neuroinvasion.

Infected monocytes are observed adhering to the endothelium of blood vessels in brain sections of infected mice (Fig. 1g, h, Extended Data Fig. 1j-l). In these adhering monocytes, *Lm*

polymerizing actin are observed, significantly more than in spleen monocytes, and occasionally adjacent to infected endothelial cells (Fig. 1h, i, Extended Data Fig. 1m-p and Video 1-3). Moreover, the transfer of monocytes infected with *Lm*Δ*actA* isogenic mutant, unable to polymerize actin and mediate cell-to-cell spread[14,15] fails to induce neuroinvasion, in contrast to the transfer of WT-*Lm*-infected monocytes infected to the same level (Fig. 1f, Extended Data Fig. 1g). Together, these results demonstrate that *Lm* accesses the brain parenchyma by ActA-mediated cell-to-cell spreading from adhering bloodborne infected inflammatory monocytes (Fig. 1j). These results are in line with previous reports obtained using poorly-neuroinvasive *Lm* strains[8,9], and suggest that neuroinvasive *Lm* strains invade the CNS in a similar manner, albeit to a far greater efficiency (up to 3 orders of magnitude) (Fig. 1a).

InlB promotes *Lm* neuroinvasion

Having identified infected monocytes as critically involved in the onset of neurolisteriosis, we looked for *Lm* factors mediating its neuroinvasiveness. Given the well-established roles of InlA and InlB in *Lm* crossing of intestinal[15] and placental barriers7, we investigated their respective role in neuroinvasion. To bypass the contribution of InlA in the crossing of the intestinal barrier, we inoculated KIE16P mice via the iv route. While InlA is not involved in neuroinvasion, InlB plays a major role: the Δ*inlB* mutant is significantly less neuroinvasive than its WT parental strain in co-infection experiments (Fig. 2a, b, Extended Data Fig. 2a-e). Accordingly, the Δ*inlAB* mutant is not less neuroinvasive than the Δ*inlB* mutant (Extended Data Fig. 2f, g), ruling out that InlA has any impact on neuroinvasion oral inoculation, a similar difference in neuroinvasiveness is observed between all representative WT strains of neuroinvasive clones and their corresponding Δ*inlB* mutant (Fig. 2c, Extended Data Fig. 2h). The involvement of InlB in neuroinvasion is also observed upon separate inoculation with either WT-*Lm* or *Lm*Δ*inlB* (Fig. 2d, e, Extended Data Fig. 2i, j). InlB contribution to neuroinvasion starts at day

3 and 4 post iv and oral inoculation, respectively, and increases over time, and *Lm*Δ*inlB* never reaches WT-*Lm* brain infection level (Fig. 2f, g, Extended Data Fig. 2k, l).

This critical role of *inlB* in *Lm* neuroinvasion was unexpected as this gene is part of *Lm* core genome and is therefore present in all *Lm* strains[17], including the poorly neuroinvasive reference strains EGDe and 10403S. Neuroinvasive *Lm* isolates actually strongly upregulate the *inlAB* operon as compared to EGDe and 10403S, both *in vitro* in liquid medium and *in vivo* in infected spleen (Fig 2h, Extended Data Fig. 2m-p). These results, together with the observation that EGDe neuroinvasion, while extremely low compared to CC4 (Fig 1a), also depends on InlB (Extended Data Fig. 2q), suggest that *Lm* neuroinvasiveness requires that InlB is highly expressed. To test this, we complemented the EGDeΔ*inlB* mutant with the *inlB* gene sequence from either EGDe or CC4 (primary sequences 93% identical, SI Table 1) in such a way that *inlB* within-host transcription levels are similar to that of endogenous *inlB* in CC4 (Extended Data Fig. 2r). These complemented strains become as neuroinvasive as WT-CC4, whereas CC4Δ*inlB* is as poorly neuroinvasive as EGDeΔ*inlB* (Fig. 2i, Extended Data Fig. 2s, t). Consistently, CC4Δ*inlB* complemented with the *inlB* allele of EGDe expressed to the level of CC4 *in vivo* is as neuroinvasive as WT-CC4 (Fig. 2i, Extended Data Fig. 2s). Altogether, these results establish that InlB overexpression is critical for *Lm* neuroinvasiveness.

We next evaluated the contribution of InlB to the infection of inflammatory monocytes, which are essential to *Lm* neuroinvasion (Fig. 1). From 3 dpi, the blood bacterial load is higher for WT-*Lm* than *Lm*Δ*inlB* (Extended Data Fig. 3a, b). Moreover, InlB significantly increases the number of *Lm*-infected inflammatory monocytes in the blood and spleen, but not the number of bacteria per infected monocyte (Fig. 2j, k, Extended Data Fig. 3c-f). Mice infected with EGDe, which expresses InlB at a significant lower level than CC4, also exhibit a lower number of infected monocytes (Extended Data Fig. 3g). In addition, WT-*Lm* is as poorly neuroinvasive as *Lm*Δ*inlB* in *Ccr2*$^{-/-}$ mice (Fig. 2l, Extended Data Fig. 3h), indicating that the contribution of

InlB to neuroinvasion implicates infected monocytes. At early time points, when equal numbers of WT and Δ*inlB*-bacteria are retrieved from the blood and brain, equivalent numbers of WT- and Δ*inlB*-infected adhering monocytes are also observed in the brain (1-2 dpi, Extended Data Fig. 1l and 3i, j), demonstrating that InlB has no impact on monocyte ability to adhere to brain vessels. Moreover, no impact of InlB on bacterial growth is detected upon direct inoculation of *Lm* into the brain (Extended Data Fig. 3k, l). Altogether, these results indicate that InlB mediates neuroinvasion by increasing the number of circulating infected monocytes, which are themselves required for *Lm* neuroinvasion.

InlB has been described as an invasion protein mediating *Lm* internalization into non-phagocytic cells[18–20]. However, entry of hypervirulent *Lm* in inflammatory monocytes, which are professional phagocytes, is InlB-independent (Extended Data Fig. 3m-o). This indicates that InlB contribution to neuroinvasion is independent of its capacity to induce internalization, and indeed InlB does not increase the number of bacteria per infected monocyte (Extended Data Fig. 3f). We therefore investigated how would InlB lead to a higher number of infected monocytes.

InlB prevents killing by CD8+ T cells

T-cell immunosuppression is a well-established risk factor for neurolisteriosis[3,21,22], and hypervirulent *Lm* clones that overexpress InlB (Fig. 2h) tend to infect patients that are the least immunosuppressed[6]. This led us to hypothesize that InlB may exhibit immunosuppressive properties. Treatment with ciclosporin, a prototypic T-cell immunosuppressant, increases neuroinvasion and renders it independent of InlB (compare Fig. 3a with Fig. 2c and Fig. 3b with Extended Data Fig. 2h), highlighting that InlB contribution to neuroinvasion is detectable only when adaptive immune responses are functional. Consistently, no difference in neuroinvasion is observed between WT-*Lm* and *Lm*Δ*inlB* before 3 dpi (Fig. 2f, g, Extended

Data Fig. 2k, l), when adaptive immune responses are not yet expected to be active[23]. Of note, ciclosporin treatment of EGDe-inoculated mice leads to a slight increase in the number of infected inflammatory monocytes and increases neuroinvasion which also becomes independent of InlB (Extended Data Fig. 4a-e). As in ciclosporin-treated mice, *Lm* neuroinvasion is increased in *Rag2*$^{-/-}$ mice lacking T- and B-lymphocytes and is fully InlB-independent (Fig. 3c, Extended Data Fig. 2k and 4d-h), demonstrating that InlB contribution to neuroinvasion requires functional lymphocytes. InlB-mediated neuroinvasion is abrogated in CD3ε$^{-/-}$ but not in muMt$^{-/-}$ mice (Fig. 3d, Extended Data Fig. 4i-k), indicating that it depends on T- but not B-lymphocytes. Indeed, CD8^{+} T-cells depletion increases *Lm* neuroinvasion and fully abrogates InlB contribution to neuroinvasion (Fig. 3e, Extended Data Fig. 4l, m). Importantly, specific anti-*Lm* CD8^{+} T-cells are induced and activated to the same extent by WT-*Lm* and its *Lm*Δ*inlB* isogenic mutant (Extended Data Fig. 5a-j), and mice inoculated with WT-*Lm* or *Lm*Δ*inlB* promote the same level of protective immunity after a second challenge (Extended Data Fig. 5k). Since *Lm* neuroinvasion (*i*) is increased in the absence of functional CD8^{+} T-cells, (*ii*) becomes InlB-independent in the absence of functional CD8^{+} T cells, (*iii*) relies on infected monocytes and (*iv*) is detectable in co-infection experiments, we reasoned that InlB may protect specifically infected monocytes from anti-*Lm* T-CD8^{+}-mediated specific killing. We therefore performed cytotoxic T-lymphocyte (CTL) assays (Extended Data Fig. 5l). Strikingly and in sharp contrast to *Lm*Δ*inlB*-infected monocytes, WT-*Lm*-infected monocytes are protected from CD8^{+} T-cells-mediated cell death (Fig. 3f, Extended Data Fig. 5m, n). Of note, the cytotoxicity mediated by CD8^{+} T-cells from either WT-*Lm* and *Lm*Δ*inlB* infected mice is similar (Fig. 3f), confirming that InlB has no impact on *Lm* immunizing capacity (Extended Data Fig. 5a-k). *In vivo*, splenic *Lm*Δ*inlB*-infected monocytes also die twice more than WT-infected monocytes (Fig. 3i). The fact that *(i*) InlB association to the bacterial surface is required for InlB-mediated neuroinvasion, (*ii*) infection of monocytes is clonal and (*iii*) InlB contribution

to neuroinvasion is detectable in co-infection experiments (Extended Data Fig. 6a-e) fully supports that InlB acts in a cell-autonomous manner.

InlB blocks Fas-mediated cell death

$CD8^+$ T-cells cytotoxicity relies on perforin-granzyme and Fas-ligand/Fas pathways[24]. InlB-mediated protection against infected monocyte killing by $CD8^+$ T-cells is fully preserved in Perforin-deficient mice (Fig. 3g). In sharp contrast, InlB inhibitory effect on infected monocytes cell death is fully abrogated in Fas-deficient mice (Fig. 3h), indicating that InlB blocks Fas-mediated killing but has no impact on the perforin pathway. Consistently, monocytes infected with WT-*Lm*, but not *Lm*Δ*inlB*, are resistant to FasL-induced cell death, whereas surface expression of Fas is not affected by InlB (Fig. 3j, Extended Data Fig. 6f, g). Accordingly, in mice treated with a pharmacological inhibitor of caspase-8, the downstream effector of Fas[25], *Lm*Δ*inlB*-infected monocytes cell death is reduced to that of WT level, and *Lm*Δ*inlB* becomes as neuroinvasive as WT-*Lm* (Fig. 3i, k, Extended Data Fig. 6h, i). WT-*Lm* infected monocytes' half-life *in vivo* is 50% longer compared to *Lm*Δ*inlB* infected cells, whereas these half-lives are equal and longer in *Rag2*$^{-/-}$ mice which lack functional lymphocytes including $CD8^+$ T-cells (Extended Data Fig. 6j). Moreover, almost 50 times more WT-*Lm*-infected monocytes than *Lm*Δ*inlB*-infected monocytes adhere to brain blood vessels (Extended Data Fig. 6k, l). In *Rag2*$^{-/-}$ mice, the same number of WT-*Lm* and *Lm*Δ*inlB*-infected monocytes circulate in the blood and adhere to the brain vessels (Fig. 3c, Extended Data Fig. 4f, g and 6k, l). Together, these results demonstrate that InlB blocks $CD8^+$ T-cells Fas-mediated killing of infected monocytes, thereby increasing their lifespan and providing them with the necessary time to adhere to brain vessels and transfer intracellular *Lm* to the brain parenchyma.

InlB blocks killing via Met/PI3Kα/FLIP

Lm-surface associated InlB mediates the recruitment of its receptor c-Met[26] both in cultured cells[27] and *in vivo* in *Lm*-infected monocytes, around bacteria both at the cell surface and intracellularly, together with the lysosome-associated membrane glycoprotein LAMP-1 and the adaptor GAB1 involved in c-Met signaling[28] (Extended Data Fig. 7a-g and Video 4, 5). This suggests that a significant fraction of InlB-mediated c-Met signaling arises from intravacuolar *Lm*, and indeed an InlB construct unable to associate to the bacterial surface and therefore unable to recruit c-Met in vacuoles, is unable to mediate neuroinvasion (Extended Data Fig. 6a-c and 7b). Consistent with a critical role of c-Met, its competitive inhibition by capmatinib fully abrogates InlB-mediated neuroinvasion (Fig. 4a, Extended Data Fig. 7h), and InlB-mediated neuroinvasion is abrogated in mice where *c-Met* is conditionally deleted in myeloid cells (*LysM*-CreER^{T2}×*Met* $^{flox/+}$ and *LysM*-CreER^{T2}×*Met* $^{flox/flox}$) (Fig. 4b, c, Extended Data Fig. 7a, i). Once activated by InlB, c-Met signals through PI3-kinase (PI3K) leading to Akt phosphorylation in infected monocytes[29,30] (Extended Data Fig. 8a, b and Video 6). InlB-mediated neuroinvasion is fully blocked by the pan-PI3K inhibitor wortmannin (Extended Data Fig. 8c-d). Specifically, the inhibition of PI3Kα (BYL-719) but not of leucocyte-specific PI3Kδ (IC87114), fully abrogates InlB-mediated neuroinvasion (Fig. 4d, Extended Data Fig. 8e, f). FLIP, a competitive inhibitor of procaspase-8 upregulated by PI3K[24,25], is upregulated in infected monocytes in an InlB dose-dependent manner, resulting in a decreased activity of caspase-8 (Fig. 4e, f, Extended Data Fig. 8g, h). Pharmacological inhibition of either c-Met or PI3Kα also limits InlB-mediated FLIP upregulation and the blocking of caspase-8 activity (Fig. 4e, f). Similarly, FLIP expression is significantly decreased in infected monocytes of *LysM*-CreER^{T2}×*Met*$^{flox/flox}$ mice, compared to littermates (Extended Data Fig. 8i), confirming genetically that c-Met is involved in InlB-mediated FLIP upregulation in infected monocytes. InlB-mediated infected monocyte resistance to cell death is lost in mice deleted for FLIP (*Rosa*-CreER^{T2}×FLIP $^{flox/flox}$, Fig. 4g, Extended Data Fig. 8j) and InlB involvement in neuroinvasion

is fully abrogated in mice conditionally deleted for FLIP in myeloid cells (*LysM*-CreER^{T2}×FLIP $^{flox/+}$ and ×FLIP $^{flox/flox}$, Fig. 4h, Extended Data Fig. 8k, l), showing that inhibition of cell death mediated by InlB-dependent FLIP upregulation is responsible for *Lm* increased neuroinvasion *in vivo*. Finally, *in vivo* exogenous activation of c-Met by its ligand hepatocyte growth factor (HGF) leads to the upregulation of FLIP expression, protects infected monocytes from cell death and renders *Lm*Δ*inlB* as neuroinvasive as WT-*Lm* (Fig 4i, Extended Data Fig. 8m-o). InlB-mediated blockade of Fas cell death pathway in infected monocytes therefore results from the InlB/c-Met/PI3Kα-dependent cell autonomous upregulation of the caspase-8 inhibitor FLIP (Extended Data Fig. 9a), which extends the half-life of infected monocytes and hence promotes neuroinvasion.

InlB promotes *Lm* intestinal persistence

InlB is part of *Lm* core genome and is under purifying selection[17,31], suggesting that InlB confers a selective advantage to *Lm*. As *Lm* is shed back from infected tissues into the intestinal lumen[32], *Lm* increased virulence may translate into increased fecal shedding and favor transmission. We therefore tested whether InlB is involved in *Lm* intestinal carriage and release in the feces upon oral and iv inoculation. Indeed, WT-*Lm* levels of infection of intestinal tissues and release in the intestinal lumen and feces are significantly higher than that of *Lm*Δ*inlB* (Fig. 4j, k, Extended Data Fig. 9b-d). At 5dpi, mouse infection by WT-*Lm* led to significantly more *lamina propria*-infected myeloid cells (CD11b$^+$ CX3CR1$^+$, more than 80% of infected cells of the intestine) than *Lm*Δ*inlB* (Extended Data Fig. 9e-g and Videos 7 and 8). As for neuroinvasion, these differences are fully dependent on CD8$^+$ T-cells, on FLIP expressed in myeloid cells and on InlB-dependent blocking of caspase-8-mediated cell death (Fig. 4k, Extended Data Fig. 10). These observations demonstrate that InlB specific interference with adaptive immunity promotes *Lm* within-host persistence and fecal shedding (Fig 4l).

Discussion

Here we uncover that *Lm* renders infected host cells resistant to $CD8^+$ T-cells-mediated killing. Selective blockade of the Fas-FasL death pathway in infected monocytes allows these cells to survive longer in the blood and to transfer *Lm* more abundantly to the brain. Importantly, this unanticipated mechanism that creates an intracellular protected niche for *Lm* is also involved in its persistence in the intestinal tissue and release in feces and ultimately the environment. This mechanism is mediated by *Lm* surface protein InlB, which was so far described as involved in *Lm* internalization into non-phagocytic cells. We have uncovered here its key role as an immunomodulatory protein. InlB promotes monocytes survival and neuroinvasion through an unsuspected mechanism: the upregulation, *via* a c-Met/PI3Kα-dependent pathway, of the competitive inhibitor of procaspase-8 called FLIP, which competitively inhibits caspase-8 cleavage and thereby blocks FasL-Fas mediated cell death.

This study highlights the critical role played by cellular immunity against intracellular pathogens' neuroinvasion from a microbial perspective. Indeed, whereas extracellular pathogens rely on the binding to specific host cell receptors[33] or the breaching of host barriers[34] to invade the CNS, the facultative intracellular pathogen *Lm* takes advantage of its ability to persist within host cells through InlB-mediated immunoresistance to favor its crossing of the blood-brain barrier *via* ActA. These results show that the capacity of microbes to survive within cells is a key pathogenic determinant favoring within-host dissemination and ultimately neuroinvasion. Other neuroinvasive intracellular pathogens such as *Mycobacterium tuberculosis* and *Toxoplasma gondii* also stimulate PI3K[35,36] and survive in myeloid cells[35,36], suggesting they may also protect infected cells from cell death, favoring their survival and increasing their within-host persistence and neuroinvasiveness.

Intracellular pathogens establish a successful infection by interfering with innate immune responses, and some also persist in the host by interfering with the adaptive immune system in

a broad and non-selective manner, like HIV, EBV and measles virus[37,38]. *Lm* has been instrumental for the discovery of cellular immunity[39] and is indeed a prototypic inducer of a protective $CD8^+$ T-cell response[40,41]. Yet, we show here that InlB selectively impairs the action of the most efficient and specific anti-*Lm* immune effector, T cells-mediated cytotoxicity, creating a protected cellular niche favoring *Lm* dissemination and persistence within the host. This is reminiscent of the mechanism by which tumor cells, in which signaling downstream of growth factor receptors is frequently constitutively activated[42,43], also evade immune responses by surviving immune killing. A detailed understanding of how microbes have selected mechanisms interfering with the immune system may help to rationally design novel anti-infective and anti-tumor therapies. Similarly, the immunomodulatory mechanism of InlB, specific and restricted to infected cells, may also help develop new immunosuppressive strategies aimed at specifically protecting cells of interest from immune killing, as opposed to classic immunosuppressive drugs that inhibit indiscriminately immune functions, which promotes infectious and neoplastic complications.

Lm is an opportunistic pathogen that only rarely induces clinically apparent infection upon oral ingestion[44], and there is no inter-human horizontal transmission of listeriosis. Yet, the so-called "virulence factors" of *Lm* are under purifying selection[17,31,45], implying that they contribute to *Lm* fitness. By interfering with the host anti-*Lm* cellular effectors, InlB enhances *Lm* intestinal carriage and fecal shedding, increasing the odds of neuroinvasive *Lm* to be transmitted back to the environment and colonize new hosts. This illustrates that the anthropocentric view on microbial pathogenesis which phenotypic output is centered on disease does not necessarily reflect the actual context where microbial evolution and fitness gain take place.

References:

1. Schuchat, A. *et al.* Bacterial Meningitis in the United States in 1995. *New England Journal of Medicine* **337**, 970–976 (1997).
2. van de Beek, D. *et al.* Clinical Features and Prognostic Factors in Adults with Bacterial Meningitis. *New England Journal of Medicine* **351**, 1849–1859 (2004).
3. Charlier, C. *et al.* Clinical features and prognostic factors of listeriosis: the MONALISA national prospective cohort study. *The Lancet. Infectious diseases* **17**, 510–519 (2017).
4. Mailles, A. & Stahl, J. Infectious Encephalitis in France in 2007: A National Prospective Study. *Clinical Infectious Diseases* **49**, 1838–1847 (2009).
5. Skogberg, K. *et al.* Clinical Presentation and Outcome of Listeriosis in Patients with and without Immunosuppressive Therapy. *Clinical Infectious Diseases* **14**, 815–821 (1992).
6. Maury, M. M. *et al.* Uncovering *Listeria monocytogenes* hypervirulence by harnessing its biodiversity. *Nature Genetics* **48**, 308–313 (2016).
7. Disson, O. *et al.* Conjugated action of two species-specific invasion proteins for fetoplacental listeriosis. *Nature* **455**, 1114–1118 (2008).
8. Drevets, D. A., Jelinek, T. A. & Freitag, N. E. *Listeria monocytogenes*-infected phagocytes can initiate central nervous system infection in mice. *Infection and Immunity* **69**, 1344–1350 (2001).
9. Join-Lambert, O. F. *et al. Listeria monocytogenes*-infected bone marrow myeloid cells promote bacterial invasion of the central nervous system. *Cellular microbiology* **7**, 167–180 (2005).
10. Cantinelli, T. *et al.* "Epidemic clones" of *Listeria monocytogenes* are widespread and ancient clonal groups. *Journal of clinical microbiology* **51**, 3770–3779 (2013).
11. Bécavin, C. *et al.* Comparison of widely used *Listeria monocytogenes* strains EGD, 10403S, and EGD-e highlights genomic variations underlying differences in pathogenicity. *mBio* **5**, e00969-14 (2014).
12. Pizarro-Cerdá, J., Lecuit, M. & Cossart, P. 8 Measuring and analysing invasion of mammalian cells by bacterial pathogens: The *Listeria monocytogenes* system. in *Methods in Microbiology* vol. 31 161–177 (Academic Press, 2002).
13. Boring, L. *et al.* Impaired monocyte migration and reduced type 1 (Th1) cytokine responses in C-C chemokine receptor 2 knockout mice. *Journal of Clinical Investigation* **100**, 2552–2561 (1997).
14. Kocks, C. *et al. L. monocytogenes*-induced actin assembly requires the actA gene product, a surface protein. *Cell* **68**, 521–531 (1992).
15. Tilney, L. G. & Portnoy, D. A. Actin filaments and the growth, movement, and spread of the intracellular bacterial parasite, *Listeria monocytogenes*. *The Journal of cell biology* **109**, 1597–1608 (1989).
16. Lecuit, M. *et al.* A transgenic model for listeriosis: Role of internalin in crossing the intestinal barrier. *Science* **292**, 1722–1725 (2001).
17. Moura, A. *et al.* Whole genome-based population biology and epidemiological surveillance of *Listeria monocytogenes*. *Nature Microbiology* **2**, 16185 (2016).
18. Gaillard, J. L., Jaubert, F. & Berche, P. The inlAB locus mediates the entry of *Listeria monocytogenes* into hepatocytes in vivo. *The Journal of experimental medicine* **183**, 359–369 (1996).
19. Braun, L. *et al.* InlB: an invasion protein of *Listeria monocytogenes* with a novel type of surface association. *Molecular microbiology* **25**, 285–294 (1997).

20. Dramsi, S. *et al.* Entry of *Listeria monocytogenes* into hepatocytes requires expression of InIB, a surface protein of the internalin multigene family. *Molecular Microbiology* **16**, 251–261 (1995).
21. Lane, F. C. & Unanue, E. R. Requirement of thymus (T) lymphocytes for resistance to listeriosis. *The Journal of experimental medicine* **135**, 1104–1112 (1972).
22. Schlüter, D. *et al.* Systemic immunization induces protective CD4+ and CD8+ T cell-mediated immune responses in murine *Listeria monocytogenes* meningoencephalitis. *European Journal of Immunology* **25**, 2384–2391 (1995).
23. Khanna, K. M., McNamara, J. T. & Lefrançois, L. In situ imaging of the endogenous CD8 T cell response to infection. *Science* **318**, 116–120 (2007).
24. Doherty, P. Cell-mediated cytotoxicity. *Cell* **75**, 607–612 (1993).
25. Muzio, M. *et al.* FLICE, a novel FADD-homologous ICE/CED-3-like protease, is recruited to the CD95 (Fas/APO-1) death-inducing signaling complex. *Cell* **85**, 817–827 (1996).
26. Shen, Y., Naujokas, M., Park, M. & Ireton, K. InIB-dependent internalization of *Listeria* is mediated by the Met receptor tyrosine kinase. *Cell* **103**, 501–510 (2000).
27. Bierne, H. *et al.* A role for cofilin and LIM kinase in *Listeria*-induced phagocytosis. *The Journal of Cell Biology* **155**, 101 (2001).
28. Weidner, K. M. *et al.* Interaction between Gab1 and the c-Met receptor tyrosine kinase is responsible for epithelial morphogenesis. *Nature* **384**, 173–176 (1996).
29. Bowers, D. C. *et al.* Scatter factor/hepatocyte growth factor protects against cytotoxic death in human glioblastoma via phosphatidylinositol 3-kinase- and AKT-dependent pathways. *Cancer Research* **60**, 4277–4283 (2000).
30. Xiao, G.-H. *et al.* Anti-apoptotic signaling by hepatocyte growth factor/Met via the phosphatidylinositol 3-kinase/Akt and mitogen-activated protein kinase pathways. *Proceedings of the National Academy of Sciences* **98**, 247–252 (2001).
31. Tsai, Y. H. L., Orsi, R. H., Nightingale, K. K. & Wiedmann, M. *Listeria monocytogenes* internalins are highly diverse and evolved by recombination and positive selection. *Infection, Genetics and Evolution* **6**, 378–389 (2006).
32. Louie, A., Zhang, T., Becattini, S., Waldor, M. K. & Portnoy, D. A. A multiorgan trafficking circuit provides purifying selection of *listeria monocytogenes* virulence genes. *mBio* **10**, (2019).
33. Coureuil, M., Lécuyer, H., Bourdoulous, S. & Nassif, X. A journey into the brain: insight into how bacterial pathogens cross blood–brain barriers. *Nature Reviews Microbiology* **15**, 149–159 (2017).
34. Devraj, G. *et al.* HIF-1α is involved in blood–brain barrier dysfunction and paracellular migration of bacteria in pneumococcal meningitis. *Acta Neuropathologica* **140**, 183–208 (2020).
35. Liu, Y., Li, J. Y., Chen, S. T., Huang, H. R. & Cai, H. The rLrp of mycobacterium tuberculosis inhibits proinflammatory cytokine production and downregulates APC function in mouse macrophages via a TLR2-mediated PI3K/Akt pathway activation-dependent mechanism. *Cellular and Molecular Immunology* **13**, 729–746 (2016).
36. Quan, J. H. *et al.* Intracellular networks of the PI3K/AKT and MAPK pathways for regulating Toxoplasma gondii-induced IL-23 and IL-12 production in human THP-1 cells. *PLoS ONE* **10**, e0141550 (2015).
37. Klenerman, P. & Hill, A. T cells and viral persistence: Lessons from diverse infections. *Nature Immunology* vol. 6 873–879 (2005).
38. Protzer, U., Maini, M. K. & Knolle, P. A. Living in the liver: Hepatic infections. *Nature Reviews Immunology* vol. 12 201–213 (2012).

39. MACKANESS, G. B. Cellular resistance to infection. *The Journal of experimental medicine* **116**, 381–406 (1962).
40. Pamer, E. G. Immune responses to *Listeria monocytogenes*. *Nature Reviews Immunology* vol. 4 812–823 (2004).
41. Shen, H. *et al.* Recombinant *Listeria monocytogenes* as a live vaccine vehicle for the induction of protective anti-viral cell-mediated immunity. *Proceedings of the National Academy of Sciences* **92**, 3987–3991 (2006).
42. Spranger, S., Bao, R. & Gajewski, T. F. Melanoma-intrinsic β-catenin signalling prevents anti-tumour immunity. *Nature* **523**, 231–235 (2015).
43. Tauriello, D. V. F. *et al.* TGFβ drives immune evasion in genetically reconstituted colon cancer metastasis. *Nature* **554**, 538–543 (2018).
44. Ricci, A. *et al. Listeria monocytogenes* contamination of ready-to-eat foods and the risk for human health in the EU. *EFSA Journal* **16**, (2018).
45. Maury, M. M. *et al.* Spontaneous Loss of Virulence in Natural Populations of *Listeria monocytogenes*. *Infection and immunity* **85**, (2017).

Fig. 1. Infected inflammatory monocytes transfer *Lm* to the CNS, by cell-to-cell spread. (**a**) Bacterial load in the brain of mice after inoculation with CC1/CC4/CC6-*Lm* and EGDe. (**b**) Bacterial load in the brain of gentamicin-treated mice after inoculation with CC4-*Lm*. (**c, d**) Three main infected cell population in the blood (c) and spleen (d) after inoculation with CC1/CC4/CC6-*Lm* in mice at 4 dpi, the peak of bacteremia (related to Extended Data Fig. 1c). For the blood, three mice are pooled together for each dot. (**e**) Bacterial load in the brain of B6-WT and *Ccr2*$^{-/-}$ mice after inoculation with CC4-*Lm*. (**f**) Bacterial load of gentamicin-treated recipient mice, 2 days after injection of infected monocytes harvested from 6 donor mice infected for 3 days with either CC4-WT or CC4Δ*actA*. (**g**, **h, i**) Representative immunofluorescence images of infected monocytes adhering to endothelial cells (g), monocytes infected by an actin-polymerizing-*Lm* (arrow) adjacent to an infected endothelial cell (arrowhead) (h), and an adhering infected monocyte (arrowhead) with actin comet-tails (i), 2 days after inoculation with CC1-*Lm* (g, h) or CC4-*Lm* (i). Maximum intensity projection over a 8µm stack (g-i). Insets are single *z*-planes (h). (**j**) Schematic representation of *Lm* neuroinvasion process.

Fig. 2. InlB is involved in *Lm* neuroinvasion and increases inflammatory monocytes infection. (**a-c**) Competition indexes in brain after inoculation with a 1:1 mix of WT and isogenic mutant strains. (**d, e**) Bacterial load in brain after inoculation with either CC4-WT or CC4Δ*inlB*. (**f, g**) Competition indexes in brain after inoculation with a 1:1 mix of CC4-WT and CC4Δ*inlB.* (**h**) Transcription levels of *inlB* relative to EGDe in infected splenocytes 2 days after iv inoculation. (**i**) Competition indexes in brain after inoculation with a 1:1 mix of the indicated bacterial strains ($2x10^4$ CFUs for EGDeΔ*inlB* / CC4Δ*inlB*). (**j, k**) Number of infected monocytes (j) and bacterial enumeration from sorted total (uninfected+infected) monocytes (k) in the blood after inoculation with CC4-WT or CC4Δ*inlB*. (**l**) Competition index in brain of

control or *Ccr2*$^{-/-}$ mice after inoculation with a 1:1 mix of CC4-WT and CC4Δ*inlB*. CFU data corresponding to competition indexes are shown in Extended Data Fig. 2 and 3.

Fig. 3. InlB blocks CD8^{+} T-cells-mediated monocyte cell death. (**a, b**) Competition indexes (a) and bacterial load (b) in brain after inoculation with a 1:1 mix of WT-*Lm* strain and Δ*inlB* isogenic mutant in ciclosporin-treated mice, related to Fig. 2c and Extended Data Fig. 2h. (**c**) Competition indexes in brain after inoculation with a 1:1 mix of CC4-WT and CC4Δ*inlB* in control and *Rag2*$^{-/-}$ mice. (**d**) Competition indexes in brain after inoculation with a 1:1 mix of CC4-WT and CC4Δ*inlB* in B6-WT and in mice lacking functional T (CD3ε$^{-/-}$), B lymphocytes (muMt$^{-/-}$) or both (*Rag2*$^{-/-}$). (**e**) Competition indexes in brain after oral inoculation with a 1:1 mix of CC4-WT and CC4Δ*inlB* after T-CD8^{+} depletion. (**f-h**) Level of caspase-3 cleavage in infected spleen monocytes, harvested from WT (f), *Prf1* KO (g), or *Fas*$^{lpr\text{-}cg}$ (h) mice, 3 days after inoculation with CC4-WT or CC4Δ*inlB*, and incubated with CD8^{+} T-cells from similarly infected (WT or Δ*inlB*) or control (PBS) mice at an effector to target ratio of 5. (**i**) Proportion of dying (Zombie-positive) infected spleen monocytes after inoculation with CC4-WT or CC4Δ*inlB* in mice treated with caspase-8 inhibitor. (**j**) Level of caspase-3 cleavage in infected spleen monocytes, harvested after inoculation with CC4-WT or CC4Δ*inlB* and treated *ex vivo* with FasL. (**k**) Bacterial load in brain after inoculation with either CC4-WT or CC4Δ*inlB* in mice treated with caspase-8 inhibitor. CFU data corresponding to competition indexes shown in Extended Data Fig. 2, 4 and 6.

Fig. 4. InlB blocks CD8^{+} T cells-mediated killing through c-Met/PI3K/FLIP, and favors *Lm* persistence in the gut. (**a**) Competition indexes in the brain after inoculation with a 1:1 mix of CC4-WT and CC4Δ*inlB*, in mice treated with a c-Met inhibitor (capmatinib). (**b, c**) Competition indexes (b) and bacterial load (c) in the brain of tamoxifen-treated *LysM*-CreER^{T2}×*Met*$^{flox/flox}$ (and *Met*$^{+/flox}$) mice (referred to as *Met*$^{LysM\Delta/\Delta}$ and *Met*$^{LysM\Delta/+}$ mice), and their

littermates, after inoculation with a 1:1 mix of CC4-WT and CC4Δ*inlB*. (**d**) Competition indexes in the brain after inoculation with a 1:1 mix of CC4-WT and CC4Δ*inlB*, in mice treated with a specific PI3Kα inhibitor (BYL-719). (**e, f**) Proportion of infected monocytes expressing FLIP (e) or active caspase-8 (f) after inoculation with CC4-WT or CC4Δ*inlB* in mice treated with either BYL-719 or capmatinib. (**g**) Level of caspase-3 cleavage in infected spleen monocytes, harvested after inoculation with CC4-WT or CC4Δ*inlB* of tamoxifen-treated *Rosa26*-CreER^{T2}×*Cflar*$^{+/flox}$ (FLIP$^{Rosa\Delta/+}$) mice and incubated with CD8^{+} T-cells from similarly infected mice at an effector to target ratio of 5. (**h**) Competition indexes in tamoxifen-treated *LysM*-CreER^{T2}×FLIP$^{flox/flox}$ (or ×FLIP$^{+/flox}$) mice (referred to as FLIP$^{LysM\Delta/\Delta}$ and FLIP$^{LysM\Delta/+}$ mice), and their littermates, after inoculation with a 1:1 mix of CC4-WT and CC4Δ*inlB*. (**i**) Bacterial load in brain after inoculation with either CC4-WT or CC4Δ*inlB* in mice treated with HGF. (**j, k**) Bacterial load in gut tissue after inoculation in KIE16P (j) and FLIP$^{LysM\Delta/\Delta}$ (k) mice with a 1:1 mix of CC4-WT or CC4Δ*inlB*. (**l**) Schematic representation of InlB-mediated blockade of CD8+ T cell-mediated cell death resulting in neuroinvasion and intestinal persistence. CFU data corresponding to competition indexes are shown in Extended Data Fig. 2, 7 and 10.

Extended Data Fig. 1. Infected inflammatory monocytes transfer *Lm* to the brain. (**a**) Bacterial load in the spleen and liver 5 days after oral inoculation with CC4-*Lm*, in mice treated with gentamicin intraperitoneally every day from day 1 post-inoculation, related to Fig. 1b. (**b**) Bacterial load in organs after iv inoculation with CC4-*Lm*, immediately followed by intravenous injection of gentamicin, assessing the bactericidal effect of gentamicin on extracellular circulating *Lm*. (**c**) Bacterial load in the blood after oral inoculation with CC1/CC4/CC6-*Lm*, related to Fig. 1a. (**d**) Repartition of the 3 main infected cell subsets in the blood and spleen after iv inoculation with CC4-*Lm*. (**e**) Number of infected inflammatory monocytes in the spleen and liver of B6-WT mice 3 days after iv inoculation with CC4-*Lm*, showing that monocytes are infected in spleen by an order of magnitude more than liver. (**f**) Number of inflammatory monocytes in the blood and spleen of B6-WT or *Ccr2*$^{-/-}$ mice. (**g**) Number of bacteria in transferred infected monocytes, harvested from spleen of mice 3 days after inoculation with CC4, related to Fig. 1f. (**h**) Schematic pipeline of the transfer experiment in *LysM*-CreER^{T2} × iDTR mice. (**i**) Bacterial load in the spleen, liver and brain of gentamicin- and diphtheria toxin-treated recipient *LysM*-CreER$^{T2+/-}$ × *Rosa26*-iDTR$^{+/-}$ and littermate mice, 4 days after injection of infected monocytes harvested from infected donor tamoxifen-treated *LysM*-CreER$^{T2+/-}$ × *Rosa26*-iDTR$^{+/-}$ or littermate mice. (**j, k**) Representative fluorescence microscopy images of brain sections with infected inflammatory monocytes adhering to endothelial cells after iv inoculation with 5×10^5 CFU CC1-*Lm*. Adhering infected cells are Ly6C$^+$ (j) and Ly6G$^-$ (k). (**l**) Number of infected monocytes adhering to brain blood vessels of mice inoculated with WT-CC4 or CC4Δ*inlB* with or without perfusion of vasculature. (**m**) Representative fluorescence microscopy image of a brain section with infected inflammatory monocytes adhering to endothelial cells after iv inoculation with 5×10^5 CFU CC1-*Lm*. Arrow: *Lm* polymerizing actin in a monocyte; arrowheads: infected monocytes. (**n**) Representative fluorescence microscopy image of splenocytes 5 days after iv inoculation with 10^4 CFU CC4-

Lm, in which intracellular *Lm* are found polymerizing actin (top insets) or in LAMP-1 positive vacuole (right insets). (**o, p**) Proportion of *Lm* detected polymerizing actin in each infected monocyte (o), or overall fraction of *Lm* associated with actin or LAMP-1 vacuoles (p) in monocytes from the spleen or from the blood vasculature of mice after inoculation with CC4-*Lm*. Values in (o) are compared with a *t*-test and proportions in (p) compared with a $\chi 2$ test. Data were obtained from two (a, l) or three (b-h, j-k, m-p) and four (i) independent experiments.

Extended Data Fig. 2. InlB expression level is a major determinant of *Lm* neuroinvasiveness, whereas InlA is not involved. (**a**) Optical density at 600 nm of indicated bacterial strains measured over time after 1:100 dilution in BHI of an overnight culture. (**b, c**) Bacterial load after oral inoculation (b) or after iv inoculation (c) with a 1:1 mix of CC4-WT expressing tdTomato or GFP. (**d**) Bacterial load in brain after iv inoculation with a 1:1 mix of WT and Δ*inlA* isogenic strains, related to Fig. 2a. (**e**) Bacterial load in brain after iv inoculation with a 1:1 mix of WT and Δ*inlB* isogenic strains, related to Fig. 2b. (**f, g**) Competition indexes (f) and bacterial load (g) in brain after iv inoculation with a 1:1 mix of CC4-WT and either CC4Δ*inlA*, CC4Δ*inlB*, CC4Δ*inlAB* or CC4Δ*inlB* complemented with *inlB* (Δ*inlB* + *inlB*), related to Fig. 2a-b and panels d, e. (**h**) Bacterial load in brain after oral inoculation with a 1:1 mix of WT strain and Δ*inlB* isogenic strains, related to Fig. 2c. (**i, j**) Bacterial load in brain after iv inoculation with 5×10^3 CFU (i) or oral inoculation with 10^9 CFU (j) of either CC4-WT or CC4Δ*inlB*. (**k, l**) Bacterial load in brain across time after iv inoculation (k) and after oral inoculation (l) with a 1:1 mix of CC4-WT and CC4Δ*inlB*, related to Fig. 2f, g. (**m**) Transcription levels of *inlA* relative to EGDe in mid-log phase in BHI. For CC1/4/6, each dot corresponds to a different clinical isolate and triangles represent the strains used throughout the rest of the study and referred to as CC1, CC4 and CC6, related to panel (o). (**n**) Transcription levels of *inlA* relative to EGDe in infected splenocytes 2 days after iv inoculation with 2×10^5 CFU in mice, related to Fig. 2h. (**o**) Transcription levels of *inlB* relative to EGDe in mid-log phase in

BHI. Each dot for CC1/4/6 corresponds to a different clinical isolate and triangles point out the strains used throughout the rest of the study and referred to as CC1, CC4 and CC6. (**p**) Representative Western blot (left) and quantification (right) of InlB expression, normalized to that of EF-Tu, relative to EGDe in mid-log phase in BHI. (**q**) Bacterial load in brain after inoculation with either WT-EGDe, EGDeΔ*inlB* and WT-CC4. (**r**) Transcription levels of *inlB*, relative to EGDe, in infected splenocytes 2 days after iv inoculation with 2×10^5 CFU of EGDe-WT, CC4-WT and strains complemented with either *inlB* from EGDe or from CC4. (**s**) Bacterial load in brain after inoculation with a 1:1 mix of the indicated bacterial strains, related to Fig. 2i. (**t**) Bacterial load in brain after inoculation with a 1:1 mix of EGDe*ΔinlB* and CC4*ΔinlB*, related to Fig. 2i. Data were obtained from three independent experiments.

Extended Data Fig. 3. InlB is not involved in *Lm* invasion of monocytes. (**a, b**) Competition indexes (a) and bacterial load (b) in blood after iv inoculation with a 1:1 mix of CC4-WT and CC4Δ*inlB.* (**c**) Number of infected monocytes in the spleen after inoculation with CC4-WT or CC4*ΔinlB*. (**d**) Bacterial load from 10^5 sorted monocytes (infected or not) retrieved from mice after inoculation with CC4-WT or CC4Δ*inlB*. (**e**) Number of infected monocytes across time in the spleen after inoculation with either CC4-WT or CC4Δ*inlB*. (**f**) Number of bacteria per infected monocyte harvested from mice after inoculation with either CC4-WT or CC4Δ*inlB.* (**g**) Number of infected monocytes in the spleen after inoculation with CC4-WT, CC4Δ*inlB* or EGDe-WT. (**h**) Bacterial load in brain of B6-WT or *Ccr2*$^{-/-}$ mice after inoculation with a 1:1 mix of CC4-WT and CC4Δ*inlB*, related to Fig. 2l. (**i, j**) Bacterial load in blood (i) and brain (j) after iv inoculation with 5×10^5 CFU of either CC4-WT or CC4Δ*inlB*. (**k, l**) Competition index (k) and bacterial load (l) in brain 1 day after intracranial inoculation with a 1:1 mix of CC4-WT and CC4Δ*inlB*. (**m-o**) Number of infected monocytes (m), percentage of infected monocytes (n) and bacterial load (o) in monocytes 1 hour after *in vitro* infection of primary bone marrow

mouse monocytes with WT-Lm or Δ*inlB* isogenic mutants, at a MOI of 5. Data were obtained from two (k-l), three (a-j) and four (m-o) independent experiments.

Extended Data Fig. 4. *Lm* neuroinvasion depends on InlB only in presence of functional CD8+ T-cells. (**a**) Number of infected monocytes in the blood and spleen of ciclosporin and gentamicin-treated mice after oral inoculation with EGDe. (**b**, **c**) Bacterial load in brain (b) and ratio of brain/blood bacterial load (c) in ciclosporin ± gentamicin-treated mice after oral inoculation with EGDe. (**d, e**) Bacterial load in brain of ciclosporin-treated mice after oral (d) and iv (e) inoculation with a 1:1 mix of EGDe-WT and EGDeΔ*inlB*. (**f, g**) Bacterial load in brain (f) and in blood (g) of *Rag2*$^{-/-}$ mice after inoculation with a 1:1 mix of CC4-WT and CC4Δ*inlB*, related to Fig. 3f. (**h**) Competition indexes in brain of *Rag2*$^{-/-}$ mice after inoculation with a 1:1 mix of WT strain and Δ*inlB* isogenic strains. (**i, j**) Bacterial load in brain (f) and in blood (g) after inoculation with a 1:1 mix of CC4-WT and CC4Δ*inlB* in control B6 WT mice and in mice lacking functional T (CD3ε$^{-/-}$), B lymphocytes (muMt$^{-/-}$) or both (*Rag2*$^{-/-}$), related to Fig. 3d. (**k**) Ratio of brain/blood bacterial loads in B6 WT, *Rag2*$^{-/-}$, CD3ε$^{-/-}$ and muMt$^{-/-}$ mice, related to Fig. 3d. (**l**) Bacterial load in brain of mice after inoculation with a 1:1 mix of CC4-WT and CC4Δ*inlB* after CD8^{+} T-cells depletion, related to Fig. 3e. (**m**) Representative dot plots (left) and proportion of CD8^{+} T-cells (right) among CD45^{+} CD3^{+} cells in the spleen, after CD8^{+} T-cells depletion, related to Fig. 3e. Data were obtained from two (m) or three independent experiments.

Extended Data Fig. 5. InlB does not alter the induction and differentiation of specific anti-*Lm* CD8^{+} T-cells. (**a, b**) Percentage (left) and number (right) of LLO-specific CD8^{+} T-cells in mesenteric lymph nodes (MLN) (a) and spleen (b) of BALB/c mice after iv inoculation with CC4-WT strain or CC4Δ*inlB*. (**c, d**) Percentage (left) and number (right) of LLO-specific CD8^{+} T-cells in MLN (c) and spleen (d) of iFABP-hEcad mice after oral inoculation with CC4-WT strain or CC4Δ*inlB*. (**e-j**) Percentage (left) and number (right) of Perforin^{+} (e), CD69^{+} (f), Granzyme-B^{+} (g), CD127^{+} (h), IFNγ^{+} (i) and KLRG1^{+} (j) CD8^{+} T-cells after iv inoculation with CC4-WT or CC4Δ*inlB*. (**k**) Bacterial load in spleen and liver after oral inoculation with CC4-

WT in mice challenged 30 days before with $5x10^7$ CFU of CC4-WT or CC4Δ*inlB*. (**l**) Schematic pipeline of the cytotoxic lymphocyte (CTL) assay. (**m**) Level of caspase-3 cleavage of infected spleen monocytes, harvested after iv inoculation with CC4-WT or CC4Δ*inlB*, and incubated with $CD8^+$ T-cells from similarly infected (WT and Δ*inlB*) or control (PBS) mice at the indicated effector to target ratio, related to Fig. 3i. Results are normalized to the level of caspase-3 cleavage in absence of $CD8^+$ T cells. (**n**) Level of caspase-3 cleavage of uninfected spleen monocytes, harvested after iv inoculation with CC4-WT or CC4Δ*inlB*, and incubated with $CD8^+$ T-cells from similarly infected (WT and Δ*inlB*) or control (PBS) mice at an effector to target ratio of 5, related to Fig. 3i. Results are normalized to the level of caspase-3 cleavage in absence of $CD8^+$ T cells. Data were obtained from three independent experiments.

Extended Data Figure 6. Membrane-associated InlB protects infected monocytes from $CD8^+$ T-cells-mediated cell death, increases their lifespan favoring their adhesion to blood brain vessels. (a) Schematic representation of WT (full length) InlB and its anchored and released variants. (**b**) Competition indexes in the brain of mice after inoculation with a 1:1 mix of CC4-WT and CC4Δ*inlB* transformed with a plasmid expressing either full-length WT InlB, cell wall-anchored InlB or released InlB. (**c**) Representative fluorescence microscopy images of centrifugated CC4Δ*inlB* transformed with a plasmid expressing either full length InlB (left panel), anchored InlB (central panel) or released InlB (right panel). Scale bars: 5 μm. (**d**) Transcription level of *inlB* in CC4Δ*inlB* transformed with a plasmid expressing InlB variants in mid-log phase in BHI, relative to CC4Δ*inlB* expressing full length InlB. (**e**) Proportion of infected monocytes containing 1 to 7 bacteria. For monocytes containing more than 1 bacteria, number of GFP- or tdTomato-expressing bacteria in each monocyte is shown. Monocytes were harvested 3 days after inoculation with a 1:1 mix of CC4-WT expressing GFP or tdTomato. **(f)** Level of caspase-3 cleavage of non-infected spleen monocytes, harvested from mice infected for 3 days with CC4-WT or CC4Δ*inlB*, incubated *ex vivo* with Fas ligand, related to Fig. 3m.

(**g**) Percentage of infected spleen monocytes expressing Fas at their surface (left), and the mean fluorescence intensity (MFI) of Fas signal (right), after inoculation with CC4-WT or CC4Δ*inlB*. (**h, i**) Competition indexes (h) and bacterial load (i) in brain after inoculation with a 1:1 mix of CC4-WT and CC4Δ*inlB* and treatment with caspase-8 inhibitor. (**j**) Proportion of dye-positive transferred monocytes among infected monocytes in the blood and the spleen after inoculation of B6 WT mice (plain lines) or *Rag2*$^{-/-}$ (dotted lines) with CC4-WT or CC4Δ*inlB*. Calculated half-lives of infected monocytes are shown in the table. (**k**) Number of infected monocytes adhering to brain vessels 2 days after inoculation with 5×10^6 CFU of CC4-WT or CC4Δ*inlB*, expressing tdTomato, of B6 WT mice immunized 2 days before with 10^3 CFU of CC4-WT expressing GFP. Each dot corresponds to the average number of monocytes counted on two slides (representative median sagittal sections, 40 μm thickness) for one mouse. (**l**) Number of infected monocytes adhering to brain vessels 2 days after inoculation with 10^6 CFU of CC4-WT and CC4ΔinlB, expressing tdTomato, of *Rag2*$^{-/-}$ mice immunized 2 days before with 10^3 CFU of CC4-WT expressing GFP. Each dot corresponds to the average number of monocytes counted on two slides (representative median sagittal sections, 40 μm thickness) for one mouse. Data were obtained from two (k,l) or three independent experiments.

Extended Data Figure 7. InlB recruits c-Met in LAMP-1+ vacuoles in infected monocytes. (**a**) Representative fluorescence microscopy images of spleen monocytes (not permeabilized) harvested from tamoxifen-treated *LysM*-CreER^{T2} × *Met*$^{flox/flox}$ (*Met* $^{LysM\,\Delta/\Delta}$) and their littermates, showing specific surface expression of c-Met. (**b**) Percentage of *Lm* co-localizing with c-Met *in vitro* in Vero cells 15 min (left), 30 min (middle) and 45 min (right) after infection at MOI 50 with CC4Δ*inlB* expressing either WT InlB, released InlB or cell wall-anchored InlB. (**c, d**) Representative fluorescence microscopy images of spleen monocytes harvested after inoculation with CC4-WT, showing intra-vacuolar *Lm* surrounded with LAMP-1 (c) and co-localizing with both c-Met and LAMP-1 (d) related to Extended Data Movie 4. (**e**)

Representative fluorescence microscopy images of spleen monocytes harvested after inoculation with CC4Δ*inlB*, showing no-colocalization with c-Met. (c-e) Maximum intensity projection over a *z*-stack. (**f**) Quantification of intracellular *Lm* co-localizing or not with c-Met and LAMP-1 in infected spleen monocytes harvested after inoculation with CC4-WT or CC4Δ*inlB*. Individual cells are plotted in top panel and samples are compared in bottom panel. (**g**) Representative fluorescence microscopy images of spleen monocytes harvested after inoculation with CC4-WT, co-localizing with both c-Met and GAB1 related to Extended Data Movie 5. Maximum intensity projection over a *z*-stack. (**h**) Bacterial load in brain after inoculation with a 1:1 mix of CC4-WT and CC4Δ*inlB* in mice treated with capmatinib, related to Fig. 4a. (**i**) Proportion of infected spleen monocytes positive for c-Met signal in flow cytometry after inoculation of $Met^{LysM\,\Delta/\Delta}$ mice and their littermates with CC4-WT. Data were obtained from three independent experiments (a, h and i) or from three microscopic field of views (f).

Extended Data Figure 8. InlB-mediated neuroinvasion involves the c-Met/PI3Kα/FLIP pathway in infected monocytes. (**a**) Representative fluorescence microscopy images of spleen monocytes harvested after inoculation with CC4-WT or CC4Δ*inlB*, showing cytosolic and nuclear phosphorylation of Akt, related to Extended Data Movie 6. Images are maximum intensity projection over a *z*-stack. (**b**) Proportion of infected spleen monocytes positive for phospho-Akt signal in flow cytometry after inoculation with CC4-WT or CC4Δ*inlB*. (**c, d**) Competition indexes (c) and bacterial load (d) in brain after inoculation with a 1:1 mix of CC4-WT and CC4Δ*inlB* in mice treated with wortmannin. (**e**) Competition indexes in brain after inoculation with a 1:1 mix of CC4-WT and CC4Δ*inlB* in mice treated with PI3Kδ inhibitor (IC87114). (**f**) Bacterial load in the brain after inoculation with a 1:1 mix of CC4-WT and CC4Δ*inlB* in mice treated with BYL-719 or IC87114, related to Fig. 4d and Extended Data Fig. 8e. (**g**) Proportion of infected spleen monocytes positive for FLIP signal in flow cytometry after

inoculation with CC4-WT, CC4Δ*inlB* or EGDe-WT. (**h**) Representative dot plot of FLIP expression in infected inflammatory spleen monocytes, after inoculation with CC4-WT or CC4Δ*inlB*, related to Fig. 4e. (**i**) Proportion of infected spleen monocytes positive for FLIP signal in flow cytometry after inoculation with CC4-WT of *Met* $^{LysM\ \Delta/\Delta}$ mice and their littermates after tamoxifen treatment. (**j**) Level of caspase-3 cleavage of infected spleen monocytes, harvested 3 days after inoculation with CC4-WT or CC4Δ*inlB* of tamoxifen-treated *Rosa26*-CreER^{T2} × *Cflar*$^{+/+}$ (FLIP$^{Rosa+/+}$) littermate mice and incubated with CD8$^+$ T-cells from similarly infected mice at an effector to target ratio of 5, related to Fig. 4g. (**k**) Proportion of infected spleen monocytes positive for FLIP signal in flow cytometry, after inoculation with CC4-WT of tamoxifen-treated *LysM*-CreER^{T2} × *Cflar*$^{flox/flox}$ (FLIP$^{LysM\ \Delta/\Delta}$) mice and their littermates (FLIP$^{LysM\ +/+}$), and after tamoxifen treatment. (**l**) Bacterial load in tamoxifen-treated (FLIP$^{LysM\ \Delta/\Delta}$), *LysM*-CreER^{T2} × *Cflar*$^{flox/+}$ (FLIP$^{LysM\ \Delta/+}$) and their littermates, after inoculation with a 1:1 mix of CC4-WT and CC4Δ*inlB* and tamoxifen treatment, related to Fig. 4h. Of note, only female mice were used for FLIP$^{LysM\ \Delta/+}$, whereas both male and female mice were included for FLIP$^{LysM\ \Delta/\Delta}$and their littermates. (**m-o**) Proportion of infected spleen monocytes positive for phospho-Akt signal (m), FLIP signal (n) and Zombie signal (o) in flow cytometry, after inoculation with CC4-WT or CC4Δ*inlB* and treatment with HGF. Data were obtained from two (m-o) or three independent experiments.

Extended Data Figure 9. In the intestinal tract, *Lm* infects CX3CR1$^+$ macrophages of the *lamina propria*, in an InlB-dependent manner. (**a**) Representation of InlB-activated pathway of infected monocytes survival to Fas-mediated cell death. (**b-d**) Bacterial load in luminal content of KIE16P (b) and B6 WT (d) or intestinal tissue of B6 WT (c) mice after oral (b) and iv (c, d) inoculation with a 1:1 mix of CC4-WT and CC4ΔinlB, related to Fig. 4j, 4k and Extended Data Fig. 10a, 10c, 10e and 10g. (**e**) Number of infected CD11b$^+$ CX3CR1$^+$ macrophages of the *lamina propria* of the small intestine of B6 WT mice in flow cytometry

after inoculation with CC4-WT or CC4Δ*inlB*. (**f, g**) Representative fluorescence microscopy images of infected CX3CR1^{+} infected macrophages in the colon *lamina propria* of mice after inoculation with CC4-WT, related to Extended Data Movies 7 and 8. Data were obtained from three independent experiments. SI = small intestine.

Extended Data Figure 10. InlB-mediated *Lm* gut persistence involves resistance to CD8^{+} T-cells and FLIP expression in myeloid cells. (**a**) Competition indexes in intestinal tissue of B6 WT and *Rag2*$^{-/-}$ mice after inoculation with a 1:1 mix of CC4-WT and CC4Δ*inlB,* related to Extended Data Fig. 9c, d and Extended Data Fig. 10b-d. (**b**) Bacterial load in intestinal tissue of *Rag2*$^{-/-}$ mice after inoculation with a 1:1 mix of CC4-WT and CC4Δ*inlB*, related to Extended Data Fig. 10a, c and d. (**c**) Competition indexes in luminal content of B6 WT and *Rag2*$^{-/-}$ mice after inoculation with a 1:1 mix of CC4-WT and CC4Δ*inlB*, Extended Data Fig. 9c, d and to Extended Data Fig. 10a, b and d. (**d**) Bacterial load in luminal content of *Rag2*$^{-/-}$ mice after inoculation with a 1:1 mix of CC4-WT and CC4Δ*inlB*, related to Extended Data Fig. 10a-c. (**e**) Competition indexes in intestinal tissue of mice after inoculation with a 1:1 mix of CC4-WT and CC4Δ*inlB* and treated with an anti-CD8^{+} T-cells antibody, related to Extended Data Fig. 9d and to Extended Data Fig.10f-h. (**f**) Bacterial load in intestinal tissue of mice after inoculation with a 1:1 mix of CC4-WT and CC4Δ*inlB* and treated with an anti-CD8^{+} T-cells antibody, related to Extended Data Fig.10 e-h. (**g**) Competition indexes in luminal content of mice after inoculation with a 1:1 mix of CC4-WT and CC4Δ*inlB* and treated with an anti-CD8^{+} T-cells antibody, related to Fig. 4j, Extended Data Fig. 9b and to panels Extended Data Fig.10e-h. (**h**) Bacterial load in luminal content of mice after inoculation with a 1:1 mix of CC4-WT and CC4Δ*inlB* and treated with an anti-CD8^{+} T-cells antibody, related to Extended Data Fig.10e-g. (**i**) Competition indexes in intestinal tissue of FLIP$^{LysM\,\Delta/\Delta}$ mice and their littermates after inoculation with a 1:1 mix of CC4-WT and CC4Δ*inlB,* related to Fig. 4k and to Extended Data Fig. 10j-m. (**j**) Bacterial load in intestinal tissue of littermates of FLIP$^{LysM\,\Delta/\Delta}$ mice after

inoculation with a 1:1 mix of CC4-WT and CC4Δ*inlB*, related to Fig. 4k, and to Extended Data Fig. 10i, k-m. (**k**) Competition indexes in luminal content of FLIP$^{LysM\ \Delta/\Delta}$ mice and their littermates after inoculation with a 1:1 mix of CC4-WT and CC4Δ*inlB*, related to Fig. 4k, and to Extended Data Fig. 10i, j, l and m. (**l**) Bacterial load in luminal content of littermates of FLIP$^{LysM\ \Delta/\Delta}$ mice after inoculation with a 1:1 mix of CC4-WT and CC4Δ*inlB*, related to Fig. 4k and to Extended Data Fig. 10i-k and m. (**m**) Bacterial load in luminal content of FLIP$^{LysM\ \Delta/\Delta}$ mice after inoculation with a 1:1 mix of CC4-WT and CC4Δ*inlB*, related to Fig. 4k and to Extended Data Fig. 10i-l. (**n, o**) Bacterial load in intestinal tissue (n) and luminal content (o) of mice after inoculation with either CC4-WT or CC4Δ*inlB* and treated with caspase-8 inhibitor, related to Fig. 3k. Data were obtained from three independent experiments. SI = small intestine.

Methods

Mice

Animal experiments were performed according to the Institut Pasteur guidelines for laboratory animals' husbandry and in compliance with European regulation 2010/63 EU. All procedures were approved by the Animal Ethics Committee of Institut Pasteur, authorized by the French Ministry of Research and registered under #11995-201703115103592 and #14644-2018041116183944.

C57BL/6JRj and BALB/c mice were purchased from Janvier Labs (France) and bred at Institut Pasteur. KIE16P mice expressing humanized E16P E-cadherin[7], iFABP-hEcad mice[16], *Rag2*$^{-/-}$ mice[46], CD3ε$^{-/-}$ mice[47], muMt$^{-/-}$[48], *Ccr2*$^{-/-}$ mice[13], CX$_3$CR1$^{+/GFP}$ [49], Rosa26CreER^{T2} [50] and Rosa26iDTR[51] were bred at Institut Pasteur. *Fas*$^{lpr-cg}$ carrying a spontaneous mutation at the Fas locus[52], and Prf1 KO mice deleted for the perforin gene[53] were obtained from Frederic Rieux-Laucat and Fernando Sepulveda, Institut Imagine, Paris, respectively. *Cflar*$^{flox/flox}$[54] (FLIP$^{f/f}$) mice were obtained from Richard M. Pope (Northwestern University, USA), Met$^{flox/flox}$ [55]from Alain Eychene (Institut Curie, Paris) and *LysM*CreER^{T2} [56] from Florian Greten (Georg Speyer Haus, Germany).

Mice were housed in groups up to 7 animals, in BSL-3 animal facility, on poplar chips (SAFE, D0736P00Z) and were fed with irradiated food at 25 kGy (SAFE, #150SP-25). The facility has central air conditioning equipment which maintains a constant temperature of 22 ± 2 °C. Air is renewed at least 20 times per hour in animal rooms. Light is provided with a 14:10 h light:dark cycle (6:30 a.m. to 8:30 p.m.). Animals were kept in polypropylene or polycarbonate cages which comply with European regulations in terms of floor surface per animal. All cages are covered with stainless steel grids and non-woven filter caps.

All experiments were performed on mice between 7 and 12 weeks of age, randomly assigned to each different condition without blinding. Unless stated otherwise in the figure legends, mice

refer to KIE16P mice. Only female mice were used throughout the study, except for experiments involving FLIP$^{flox/flox}$ x *LysM*CreER^{T2} and Met$^{flox/flox}$ x *LysM*CreER^{T2} mice for which both male and female mice were included.

No sample size calculations were performed. The sample size (n) of each experiment is provided in Supplementary Information Table 7 for the main figures and also on each panel as each dot corresponds to one mouse/sample. Sample sizes were chosen to support meaningful conclusions with the statistical tests used. We used around 8 to 14 mice per group, a number sufficient to reach statistical significance using non-parametric statistical tests with the effect size we expected to observe, based on our previous observations.

Bacterial strains

All bacterial strains used in this study are presented in Supplementary Information Table 2. To obtain growth curves, bacteria grown overnight in BHI (with chloramphenicol when needed), at 37°C and 200 rpm, were diluted 1:100 in BHI (with chloramphenicol when needed), incubated at 37°C and 200 rpm, and OD_{600} was measured every hour for 9 hours. Growth curves were fitted using Gompertz model to compare parameters between each strain.

Mutagenesis and plasmids

The oligonucleotide primers and plasmids used in this study are listed in Supplementary Information Table 3 and 4, respectively. Deletion mutants were constructed as described by Monk et *al.*[57] The flanking regions of the target genes were PCR amplified. After purification, the fragments were stitched together by sequence overlap extension then cloned into the pMAD shuttle vector[58]. The vector was then electroporated into electrocompetent *Lm* cells. After plasmid integration and excision by sequence homology, gene deletion was verified by sequencing the PCR product of the target region. For *Lm*Δ*inlA* mutants, to avoid alteration of

InlB expression in the operon, the *inlA* gene with flanking regions was PCR amplified and cloned into pLR16-pheS plasmid[59] (kind gift from Prof. Anat Herskovits, Tel Aviv University) and a point mutation was introduced via PCR in the *inlA* gene resulting in a premature stop codon. The plasmid was then purified and electroporated into electrocompetent *Lm*Δ*inlA* bacteria. After plasmid integration and excision by sequence homology, allele replacement was verified by sequencing the PCR product of the target region.

The pAD backbone[60], integrated as a single copy at the tRNAArg-attBB site into *Listeria* genome, was used to allow expression of tdTomato and GFP. First an EcoRV restriction site was added in pAD between the 5'UTRhly and the ATG start codon, generating the plasmid pCMC12. TdTomato and GFP sequences were codon-optimized for expression in *Lm* using Optimizer (http://genomes.urv.es/OPTIMIZER/), synthesized by Eurofins with EcoRV and SalI flanking restriction sites and inserted in pCMC12 between EcoRV and SalI sites. *inlB* sequences were amplified from EGDe (MBHL0005), CC4 (MBHL0257) and *Listeria innocua* BUG1642 (MBHL0052, expressing a construct where InlB anchoring region has been replaced by the anchoring domain of *S. aureus* protein A[19]) genomic DNAs and were inserted in pCMC12 between EcoRV and SalI sites. The promoter in pCMC12 is pHyper, a strong constitutive promoter that allows an *in vivo* expression level of InlB in complemented strains equivalent to that of hypervirulent strains. The β-lactamase construct was described in Quereda et *al*.[61] All constructs were electroporated into electrocompetent *Lm* cells. Integration was verified by PCR.

Infections and bacterial enumerations

Bacterial inocula were prepared by centrifugation of a bacterial culture grown in BHI, at 37°C and shaken at 200 rpm, until OD_{600} of 0.8 (8.10^8 viable bacteria per mL), washed in PBS and resuspended in PBS at the appropriate dilution. For oral inoculation, 0.2 mL of bacteria ($2x10^8$

CFUs, unless specified otherwise) were mixed to 0.3 mL of PBS containing 50 $mg.mL^{-1}$ of $CaCO_3$ (Sigma) and injected intragastrically via a feeding needle (ECIMED) to isoflurane-anesthetized mice. For intravenous infection, 0.1 mL of bacteria (10^4 CFUs, unless specified otherwise) were injected in the tail vein using a 25G needle.

For intracerebral infections, mice were anesthetized in 3% isoflurane, then received 10 µl of bacterial suspension by intracranial injection using a 26G needle, inserted approximately 2 mm anterior to the bregma, 1 mm laterally and 1.5 mm ventrally, corresponding to the frontal motor cortex as it is the most easily accessible part of the brain for reproducible intracranial inoculation, and as it avoids major blood vessels.

For immunization experiments, mice were first infected with WT or Δ*inlB* strains by oral gavage with 5.10^7 CFU. After 30 days, mice were then infected intragastrically for the second challenge with 2.10^9 WT bacteria for 3 days.

At indicated times, mice were euthanized, either through CO_2 exposure, or ketamine/xylazine overdose and transcardial perfusion when flushing of the vasculature was necessary (Extended Data Fig. 1l). Organs were aseptically harvested. Intestine, colon and cæcum were incubated with gentamicin 100 µg/mL for 2 hours to eliminate extra-tissular bacteria. All organs were homogenized in PBS with a tissue homogenizer (UltraTurrax T-25 basic, IKA works). Serial dilutions of the homogenate were plated onto BHI agar (or ALOA for feces and intestinal content) and CFUs enumerated. CFUs are expressed per mL for blood and per whole organ otherwise. CFUs in brain comprises both CFUs in parenchyma and in meninges.

Competition index experiments were performed as described in Disson *et al*.[62] Briefly, a 1:1 ratio of wild-type bacteria, expressing TdTomato, and mutant bacteria, expressing GFP, was injected into mice, confirmed by CFUs enumeration of the inoculum onto BHI agar. WT and mutant bacteria CFUs were distinguished by colonies' color onto BHI agar. Competition index is calculated as the ratio of WT versus mutant CFUs in each organ. Mice with a bacterial load

lower than 10 CFUs were not included for calculation of competition indexes, as it may induce a bias, but are presented in the corresponding CFU graphs to show the global level of neuroinvasion. Except stated otherwise, competition indexes were performed 5 days post-inoculation, a time point late enough to have consistent CNS invasion and induction of adaptive immune responses but before humane endpoints were reached. Whenever the mouse strains were permissive to *Lm* oral infection, intragastric inoculation was used for competition index assays.

Drug treatments of mice

All drugs used in this study and their mode of delivery are presented in Supplementary Information Table 5.

Gentamicin was administered intraperitoneally every day from 1 dpi to assess the contribution of intracellular bacteria to brain infection, except in Extended Data Fig. 1b where it was intravenously injected immediately after iv infection with extracellular *Lm,* to demonstrate gentamicin bactericidal effect on extracellular bacteria.

For *in vivo* hepatocyte growth factor (HGF) administration, due the extremely short half-life of HGF, recombinant mouse HGF (Biolegend) was administered using a micro-osmotic pump (Model 1003D, Alzet), inserted subcutaneously under isoflurane anesthesia as described previously[63]. The pumps were loaded with 100 µL of mHGF in PBS (150 µg/mL) or PBS alone with a delivery rate of approximately 1 µL/hour over a 3 days period.

RNA isolation and qRT-PCR

For *in vitro* analysis, bacteria were grown in BHI at 37°C and 200 rpm until OD_{600} 0.8. They were then centrifuged, lysed in resuspension buffer (10% glucose, 12.5 mM Tris, 10 mM EDTA in nuclease-free water), transferred into Precellys tube (Ozyme) containing 0.1 mm ceramic beads (Ozyme) and acid phenol (Sigma) and homogenized using a Precellys 24 apparatus

(Ozyme). Aqueous phase was transferred into a new tube containing TRIzol (Invitrogen) and chloroform (Sigma), shaken and centrifuged at maximum speed at 4°C for 15 min. Aqueous phase was transferred into a new tube containing chloroform, shaken and centrifuged at maximum speed at 4°C for 15 min. Aqueous phase was transferred into a new tube containing 1 volume of isopropanol (Sigma) and 0.1 volume of 3M sodium acetate (Sigma), incubated for at least 20 min at -20°C.

For *in vivo* analysis, spleens were harvested aseptically, and single cells suspensions were obtained by homogenizing through a 40 μm cell strainer. Cells were lysed in TRIzol and chloroform, shaken and centrifuged at maximum speed at 4°C for 15 min. Aqueous phase was transferred into a new tube containing 1 volume of isopropanol, incubated for at least 20 min at -20°C.

Both for *in vitro* and *in vivo* samples, RNAs were pelleted at maximum speed at 4°C for at least 20 min and washed three times in 80% ethanol (Sigma), air-dried and dissolved in RNase-free water. Total RNA was reverse-transcribed using hexameric random primers (Invitrogen) and M-MLV reverse transcriptase (Invitrogen) following manufacturer's instructions. Quantification of gene expression was performed using Power SYBR^{TM} Green PCR Master Mix, a Step-One Real-Time PCR apparatus (both from Applied Biosystems) and primers listed in Supplementary Information Table 3. Expression of *inlA* and *inlB* was normalized to that of *gyrB* and compared to EGDe using the ΔΔCt method.

Flow cytometry

Mice were euthanized at the indicated times post-infection. Functional characterization of $CD8^+$ T cells and infected monocytes were performed after iv inoculation, unless stated otherwise, which allows for less intra-animal variation and thus reduces the number of animals needed for experiments. Counting and characterization of infected cells in the blood and spleen were

performed at 4 days post-inoculation (both orally and iv), when bacteremia is the highest. For orally infected mice, the bacteremia being very low even at 4 days post-inoculation, blood of 3 mice was pooled and analyzed as one sample. Counting and characterization of infected cells in the intestine was performed after iv inoculation, to avoid early infection events linked to the inoculum passage of the intestinal barrier after oral inoculation, at 5 days post-inoculation, a time when the bacterial load is sufficient to detect late infection events. For cell death-related experiments and characterization of infected inflammatory monocytes, we harvested spleen at 3 dpi, the earliest timepoint at which the effect of InlB is consistently observed, but also when cell death is moderate in the spleen, so that we could harvest sufficient number of viable cells. Spleens, livers, mesenteric lymph nodes (MLN) and blood (by cardiac puncture in heparin-coated syringe) were harvested aseptically. Single cells suspensions were obtained from spleen and MLN by homogenizing through a 40 μm cell strainer. Single cells suspensions were obtained from liver using the Multi Tissue Dissociation Kit 1 (Miltenyi Biotec) and MACS apparatus (Miltenyi Biotec) following the manufacturer's instructions and successive filtration through 70 and 40 μm cell strainer. After red blood cells lysis using 1X RBC lysis buffer (eBiosciences), cells were washed in Cell Staining Buffer (CSB) (BioLegend) before further processing.

Small intestines were harvested without conjunctive tissue, opened longitudinally, washed in ice-cold PBS and cut into 1-1.5 cm pieces and washed again in ice-cold PBS. Epithelial cells were first isolated after incubation of intestinal pieces in HBSS (Invitrogen) with 5% fetal calf serum, 10mM HEPES (Sigma) and 5mM EDTA for 3 times 20 min at 37°C with 200 rpm shaking. After washing in ice-cold DMEM (Invitrogen), leukocytes of the *lamina propria* were isolated after incubation in DMEM with DNase I (Roche) and Liberase TL (Roche) for 45 min at 37°C with 200 rpm shaking. Single cells suspensions of epithelial cells and leukocytes from

the *lamina propria* were filtered successively through 100, 70 and 40 µm cell strainer, washed in ice-cold DMEM, then in CSB and processed further separately.

If required, cells were labeled using the LiveBLAzer^{TM} FRET-B/G Loading Kit with CCF2-AM (Invitrogen), a fluorescent substrate of β-lactamase that can cross the plasma membrane. Presence of β-lactamase-expressing bacteria in cells induces a shift in the fluorescence emission of the CCF2-AM substrate from 518 nM (green) to 447 nM (blue) upon excitation with the 405 nM laser and thus allows for identification of infected cells. Cells were loaded with the CCF2-AM substrate following manufacturer's instructions for 2h30 at room temperature in CSB containing 1mM probenecid (Sigma). After washing, cells were blocked using CD16/32 (BioLegend) for 5 min at room temperature, washed in CSB, stained with the appropriate antibodies (listed in Supplementary Information Table 6) for 45 min at 4°C and washed in CSB. If no intracellular staining was required, cells were suspended in CSB containing CountCAL beads (Sony) for absolute counting of cells. For intracellular staining, cells were fixed for 20 min at room temperature in IC fixation buffer (eBiosciences), washed three times in 1X permeabilization buffer (eBiosciences), incubated with primary antibodies for 1 hour at room temperature, washed and incubated with secondary antibodies for 45 min at room temperature. After washing, cells were suspended in CSB containing CountCAL beads for absolute counting of cells. Cells were acquired on a Fortessa X-20 SORP apparatus (BD biosciences) and analyzed using FlowJo software (TreeStar). B-cells were defined as $CD45^+$ $CD19^+$ $CD3^-$; $CD8^+$ T-cells as $CD45^+$ $CD3^+$ $CD8^+$ $CD19^-$; LLO-specific $CD8^+$ T-cells as $CD45^+$ $CD3^+$ $CD8^+$ LLO-pentamer$^+$ $CD19^-$; $CD4^+$ T-cells as $CD45^+$ $CD3^+$ $CD4^+$ $CD19^-$; granulocytes as $CD45^+$ $Ly6G^+$ $CD3^-$ $CD19^-$; patrolling monocytes in blood as $CD45^+$ $CD11b^+$ $CD11c^+$ $CD3^-$ $CD19^-$ $Ly6G^-$ $Ly6C^-$; inflammatory monocytes as $CD45^+$ $CD11b^+$ $Ly6C^{high}$ $CD3^-$ $CD19^-$ $Ly6G^-$ $CD11c^-$; macrophages in spleen as $CD45^+$ $CD11b^+$ $CD11c^+$ $CD3^-$ $CD19^-$ $Ly6G^-$ $Ly6C^-$; dendritic cells in spleen as $CD45^+$ $CD11c^+$ $CD3^-$ $CD19^-$ $Ly6G^-$ $Ly6C^-$; macrophages in *lamina propria* as

$CD45^+$ $CD11b^+$ $CX3CR1^+$ $CD3^-$ $CD19^-$ $Ly6G^-$ $CD11c^-$; dendritic cells in *lamina propria* as $CD45^+$ $CD11c^+$ $CD103^+$ $CD3^-$ $CD19^-$ $Ly6G^-$ $Ly6C^-$; epithelial cells in the intestine as Ep-Cam^+ $CD45^-$; dying cells as Zombie NIR^+; infected cells as CCF2-blue and non-infected cells as CFF2-green. Number of cells are expressed per mL of blood, per spleen or per small intestine.

CTL assays

Infected mice were euthanized 3 days post-infection, a time point where activated $CD8^+$ T cells are already present but prior to cell death induced in infected monocytes. Spleens were harvested aseptically and cells prepared as described above for flow cytometry, resuspended in CSB and sorted on a FACSAria III apparatus (BD Biosciences) into fetal calf serum-containing tubes. Activated $CD8^+$ T-cells were defined as $CD45^+$ $CD3^+$ $CD8^+$ $CD69^+$ $CD19^-$, infected inflammatory monocytes as $CD45^+$ $CD11b^+$ $Ly6C^{high}$ $CD3^-$ $CD19^-$ $Ly6G^-$ $CD11c^-$ CCF2-blue and non-infected inflammatory monocytes as $CD45^+$ $CD11b^+$ Ly-$6C^{high}$ $CD3^-$ $CD19^-$ $Ly6G^-$ $CD11c^-$ CCF2-green. For mock-treated mice, $CD8^+$ T-cells and inflammatory monocytes were sorted. After sorting, cells were washed and resuspended in RPMI medium (Invitrogen) containing 10% fetal calf serum. Activated $CD8^+$ T-cells and monocytes (infected and non-infected), isolated from independent mice, were co-incubated at the indicated ratio for 80 minutes at 37°C, washed and fixed with IC fixation buffer overnight at 4°C. After three washes in 1X permeabilization buffer, cells were stained with anti-cleaved caspase-3 antibody for 1 hour at room temperature, washed and stained with secondary antibody for 45 minutes at room temperature. After washing, cells were acquired on a X-20 Fortessa SORP apparatus and percentage of monocytes positive for cleaved caspase-3 signal analyzed using FlowJo software.

Infected monocytes half life

Mice (B6 WT or *Rag2*$^{-/-}$) were infected intravenously with 10^4 *Lm* CFUs. At day 2 post inoculation, single cells suspensions were obtained from spleens of non-infected B6 WT mice as described in the flow cytometry section. Cells were then labelled with Vybrant DiD solution (Invitrogen™) for 20 minutes at 37°C, according to the manufacturer's instructions. After 3 washes in DMEM-F12 medium, cells were resuspended in PBS and immediately transferred into infected mice intravenously, where they could get infected. Mice were euthanized at indicated time points, starting from 12h post-transfer (arbitrarily defined as time 0) in order to let time for transferred monocytes to be infected *in vivo* in sufficient numbers to be readily detected before assessing their decay. Spleen and blood samples were harvested aseptically. Single cells suspensions were then prepared and loaded with the CCF2-AM substrate and stained as described above. After washing, cells were acquired on a X-20 Fortessa SORP apparatus and the percentage of infected monocytes positive for Vybrant DiD signal was analyzed using FlowJo software.

Estimation of infected monocytes half-lives from exponential fits

The proportion of infected transferred monocytes (relative to their number at timepoint 0) in the spleen and blood of recipient mice across time were fitted by a one-phase decay exponential function ($y = K \times \exp(-t/\tau)$). Half-lives were determined as $t_{1/2} = \ln(2)/\tau$, using the τ values from the best-fit parameters for each condition. Values of half-lives were then compared using the extra-sum of squares *F*-test, and the corresponding *p*-values reported in the figure.

Fas ligand treatment

Infected mice were euthanized 3 days post-infection and spleens were harvested aseptically. Cells were prepared and sorted in the same conditions as for CTL assays. Infected and non-infected inflammatory monocytes were sorted into fetal calf serum-containing tubes. After

sorting, cells were washed and resuspended in RPMI medium containing 10% fetal calf serum. Cells were then treated with either HA antibody as control (Cell Signaling) or with HA antibody plus recombinant mouse Fas ligand/TNFSF6 (R&D systems) for 80 minutes at 37°C. After washing, cells were fixed overnight in IC fixation buffer. After three washes in 1X permeabilization buffer, cells were stained with anti-cleaved caspase-3 antibody for 1 hour at room temperature, washed and stained with secondary antibody for 45 minutes at room temperature. After washing, cells were acquired on a X-20 Fortessa SORP apparatus and percentage of monocytes positive for cleaved caspase-3 signal analyzed using FlowJo software.

Caspase 8 activity assay

Mice were inoculated intravenously, treated with either BYL-719 or Capmatinib and euthanized at 3 days post-infection. Single cells suspensions were prepared from spleen as described in the flow cytometry section. After CCF2-AM loading, blocking with CD16/32 and staining with the appropriate antibodies, cells were incubated for 30 min at 37°C with Red-IETD-FMK from CaspGLOW^{TM} Red Active Caspase-8 Staining Kit (Clinisciences), washed and suspended in Wash buffer containing CountCAL beads for absolute counting of cells. Cells were immediately acquired on a Fortessa X-20 SORP apparatus and analyzed using FlowJo software.

Transfer into recipient mice of infected monocytes

Infected KIE16P mice were euthanized 3 days post-infection and spleens were harvested aseptically. Cells were prepared as described above and sorted in the same conditions as for CTL assays. Infected monocytes from 6 mice were sorted into fetal calf serum-containing tubes, pooled, washed and injected into a naïve mouse treated with gentamicin, corresponding to an

inoculum of 10^4 live CFUs. Two days post-injection, the mouse was euthanized, organs harvested aseptically and bacteria enumerated as described above.

LysM-CreER$^{T2+/-}$ × *Rosa26*-iDTR$^{+/-}$ and their littermates were infected intravenously with CC4-*Lm*, treated with tamoxifen to allow for Cre expression, euthanized 4 days after infection and spleens harvested aseptically. Cells were prepared as described above and sorted in the same conditions as for CTL assays. Infected monocytes from 3 mice were sorted into fetal calf-serum containing tubes, pooled (corresponding to an inoculum of $2x10^4$ live CFUs), washed and injected into a naïve recipient mouse (same genotype as donor mice) treated with both diphtheria toxin and gentamicin, to kill Cre-expressing monocytes and extracellular bacteria. Four days post-injection, mice were euthanized, organs harvested aseptically and bacteria enumerated as described above.

Bacterial enumeration in infected monocytes

Infected mice were euthanized 4 days post-infection, when the bacteremia is the highest, and spleens and blood were harvested aseptically. Cells were prepared as described above and sorted in the same conditions as described for CTL assays. Monocytes were collected into fetal calf serum-containing tubes, washed and resuspended into 0.1% triton, serially diluted in PBS and plated on BHI agar.

Immunofluorescence labelling and fluorescence microscopy

Brain hemispheres were fixed in 4% paraformaldehyde in PBS overnight at 4°C then washed in PBS, embedded in 4% agarose and sectioned into 40 µm-thick slices using a vibrating microtome (ThermoScientific, HM 650V).

Slices were washed in PBS then incubated for 2 hours in blocking-permeabilization solution (10% goat serum, 4% fetal calf serum and 0.4% Triton X-100 in PBS). Tissues were then

labeled with the appropriate primary antibodies (listed in Supplementary Information Table 6) overnight at 4°C in mild blocking conditions (4% goat serum, 4% fetal calf serum and 0.4% Triton X100 in PBS), washed in PBS, then incubated with secondary antibodies (listed in Supplementary Information Table 6), Hoechst-3342 and Phalloidin-Alexa 647 for 2 hours at room temperature. Tissues were washed in PBS and then mounted on glass slides under coverslips in mounting medium (Invitrogen). The slides are let in obscurity overnight before observation under a Zeiss LSM900, LSM710 or LSM700 microscope and acquisition with the ZEN software. 3D reconstruction were performed using the Arivis Vison 4D software.

For gut and spleen sections microscopy, mice were infected with 5.10^3 CFUs and euthanized 5 days post-iv inoculation. iv allowed to observe only late infection events in the intestine (and not infection events linked to the inoculum as for oral inoculation). Spleen, small intestine and colon were harvested without conjunctive tissue, washed in ice-cold PBS and fixed in 4% paraformaldehyde in PBS overnight at 4°C then washed in PBS, embedded in 4% agarose and sectioned into 70 μm-thick slices using a vibratome. Slices were washed in PBS then incubated for 2 hours in blocking-permeabilization solution (3% bovine serum albumin and 0.4% Triton X-100 in PBS). Tissues were then labeled with the appropriate primary antibodies (listed in Supplementary Information Table 6) overnight at 4°C in mild blocking conditions (3% bovine serum albumin and 0.4% Triton X100 in PBS), washed in PBS, then incubated with secondary antibodies (listed in Supplementary Information Table 6), Hoechst-3342 and Phalloidin-Alexa 647 when indicated for 2 hours at room temperature. Tissues were washed in PBS and then mounted on glass slides under coverslips in mounting medium. The slides are let in obscurity overnight before observation under a Zeiss LSM900 or LM710 microscope and acquisition with the ZEN software. 3D reconstruction were performed using the Arivis Vison 4D software.

For monocytes microscopy, sorted monocytes were seeded on poly-D-lysine-coated 96 wells-plates or on Nunc® Lab-Tek® Permanox slides, fixed in 4% paraformaldehyde in PBS overnight

at 4°C and then washed in PBS. Cells were then permeabilized in 0.1% Triton X-100 for 10 minutes, incubated with blocking solution (5% BSA in PBS) for 30 minutes at room temperature, then labeled with anti-*Lm* antibody for 1 hour at room temperature in PBS-BSA, washed in PBS, and then incubated with anti-rabbit secondary antibody, Hoechst-3342 (ThermoFisher) and Phalloidin-Alexa 647 (ThermoFisher) for 1 hour at room temperature. For total c-Met staining, cells were incubated with anti-c-Met in mild blocking conditions (2.5% BSA, 0.2% Triton X-100 in PBS) overnight at 4°C, washed in PBS and incubated with anti-*Lm* overnight at 4°C. For p-Akt and LAMP-1 staining, cells were labelled with primary antibodies solution (anti p-Akt or anti LAMP-1 and anti-*Lm*) in mild blocking conditions (2.5% BSA, 0.2% Triton X-100 in PBS) overnight at 4°C then washed in PBS. Cells were then incubated with appropriate secondary antibodies solution (see Supplementary Information Table 6) and Hoechst-3342 for 2h at room temperature, washed in PBS and left in PBS at 4°C (96 wells plates) or covered by mounting medium and a coverslip (Nunc® Lab-Tek® Permanox slides). For labeling of membrane accessible c-Met, unpermeabilized cells were incubated with blocking solution (5% BSA in PBS) for 30 minutes at room temperature, then labeled with anti-c-Met in blocking solution without Triton X-100 overnight at 4°C, washed in PBS and incubated with anti-Goat-Alexa 546 in 5% BSA in PBS. Cells were then washed in PBS, permeabilized in 0.1% Triton X-100 and incubated with anti-CD11b in blocking solution (2.5% BSA, 0.2% Triton X-100 in PBS) for 2h at room temperature, washed in PBS, incubated with anti-Rat-Alexa 488 and Hoechst-3342 for 2h at room temperature, washed in PBS and left in PBS at 4°C (96 wells plates) or covered by mounting medium and a coverslip (Nunc® Lab-Tek® Permanox slides). Cells were observed under a Zeiss LSM900 or LM710 microscope and images acquired with the ZEN software. 3D reconstruction were performed using the Arivis Vison 4D software.

For microscopy of BHI grown-bacteria, 50 µL of the overnight culture were diluted in 1 mL PBS, spun down in a microfuge for 2 minutes, fixed in 4% paraformaldehyde in PBS for 15 minutes at room temperature then washed in PBS. Bacteria were then permeabilized using 0.5% Triton X100 for 10 min, washed in PBS, then incubated with blocking solution (1% BSA in PBS) for 30 minutes. Next, bacteria were labelled with anti-InlB primary antibody in blocking solution (1% BSA in PBS) for 1 hour at room temperature, washed 3 times in PBS, then incubated with anti-rabbit secondary antibody for 1h at room temperature. After 3 washes in PBS, bacteria were resuspended in Hoechst solution (dilution 1/5000 in PBS) for 15 minutes at room temperature, washed twice with PBS then resuspended in 4 µL PBS. Finally, the bacterial suspension was loaded onto a glass slide coated with 1% agarose gel and a coverslip before observation under a Zeiss LM710 microscope and acquisition with the ZEN software.

Adhering infected monocytes quantification

For microscopy quantification of infected monocytes adhering to the brain vasculature, mice were inoculated by iv with high inocula (5.10^5 – 5.10^6 CFUs) and euthanized after 2 days, a time point with enough crossing events to allow analysis but without damages to the blood-brain barrier. As mice reach humane endpoint in 2 days with this high inoculum, to quantify the dynamics of infected monocytes recruitment to brain blood vessels when the adaptive immune response starts to act (> 2dpi), we inoculated mice first by iv with 10^3 CFU of GFP-*Lm*, and again 2 days later with 10^6-5.10^6 CFU of tdTomato-*Lm*. This allowed to induce a high-level infection, necessary to detect *Lm*-tdTomato-infected monocytes in the brain vasculature, during a time window (from 2 to 4 dpi) when the adaptive immune response is developing, and when WT-infected monocytes have a lifespan 50% longer than Δ*inlB*-infected ones in mice with a functional adaptive immune system (half-life experiments, Extended Data Fig. 6j). Quantification was performed on a 40µm-thick medio-sagittal brain section. The number of

Ly6C+ infected cells observed adhering to brain blood vessels (visualized by Ly6C and actin staining) on the whole tissue section was quantified. The mean value of 2 sections per mouse is reported in the figures.

Immunoblotting

To assess InlB expression level, bacterial cultures at OD_{600} of 0.8 were centrifuged at 3000 g for 10 minutes. Pellets were then incubated with B-PER™ Complete Bacterial Protein Extraction Reagent (ThermoFisher Scientific) for 15 minutes at room temperature and centrifuged at 16,000 g for 20 minutes to obtain lysates.

Lysates were mixed with reducing sample buffer (NuPAGE, Invitrogen) for electrophoresis and subsequently transferred onto a nitrocellulose membrane. Membranes were then blocked with 5% non-fat milk diluted in PBS Tween 0.1 % for 1 hour and incubated with primary antibodies in blocking solution for 2 hours at room temperature. After 1 hour of secondary antibody incubation, immunodetection was performed by using a chemiluminescence kit (Amersham™ ECL™ Prime, GE Healthcare), and bands were revealed using the PXi imaging system (SYNGENE). All uncropped immunoblots are included in Supplementary Information Fig.1.

***In vitro* monocytes infection assays**

C57BL/6JRj mice were euthanized and bone marrow was collected aseptically. Cells were washed in PBS, red blood cells lysed as described in the flow cytometry section and monocytes isolated using the mouse Monocyte Isolation Kit (Miltenyi Biotec) following manufacturer's instructions. Cells were incubated overnight at 37°C in RPMI + 10% fetal calf serum and penicillin/streptomycin, washed in RPMI, plated in 96 wells-plate, infected with GFP-expressing *Lm* at MOI 5 for 1 hour at 37°C and treated with 50 µg/mL gentamicin for 1 hour at

37°C. For bacterial enumeration, cells were washed in PBS, lysed in 0.1% triton, serially diluted in PBS and plated onto BHI agar. For flow cytometry analysis, cells were washed, fixed in IC fixation buffer in presence of CountCAL beads, acquired on a X-20 Fortessa SORP apparatus and analyzed using FlowJo software.

In vitro infection of Vero cells

Vero cells (ATCC® CCL-81™) were directly purchased from ATCC who performed authentication and were negative for mycoplasma contamination. Vero cells were seeded on poly-D-lysine-coated 96 wells-plates in DMEM (Invitrogen) + 5% fetal calf serum and penicillin/streptomycin 24 hours prior to infection. On the day of infection, cells were washed three times in DMEM + 0.2% fetal calf serum and incubated in this medium for four hours. Bacteria grown in BHI at 37° and 200 rpm until OD_{600} 0.8 were centrifuged, washed in PBS, suspended in DMEM and added to the cells at a MOI of 50. After 1 min centrifugation at 200 g, cells were incubated at 37° for the indicated times, fixed for 15 min in 4% PFA and washed three times in PBS. Staining for microscopy was performed as for sorted monocytes in the above section.

Statistical analyses

Analyses were performed using GraphPad Prism 8 Software. Number of independent experiments performed for the main figures are found in Supplementary Information Table 7 and in the corresponding legends for Extended Data Figures. Each dot corresponds to one mouse/one sample, unless stated otherwise. All statistical tests were two-sided. All data are presented as median ± interquartile (box) and extreme values (lines) or as median ± interquartile (Fig. 1a; ED Fig. 1c, p; ED Fig. 6j), mean ± SD (Fig. 2h; Fig.3f-h, j; Fig. 4g; ED Fig. 1l; ED Fig. 2a, m-p, r; ED Fig 5m, n; ED Fig. 6d, g; ED Fig. 8b, j), mean (ED Fig 1p; ED Fig. 6e, ED

Fig. 7b), and violin plot (ED Fig. 3f). CFU are compared with the unpaired Mann-Whitney test (2 samples) or Kruskal-Wallis test with Dunn's post hoc test (more than 2 samples). CFU in competition assays are compared with the Wilcoxon matched-pairs signed rank test and competition indexes are compared with the unpaired Mann-Whitney test (2 samples) or Kruskal-Wallis test with Dunn's post hoc test (more than 2 samples). Number of infected cells are compared with unpaired Mann-Whitney test (2 samples), Kruskal-Wallis test with Dunn's post hoc test (more than 2 samples) or with the Friedman test with Dunn's post hoc test (Fig. 1c and d; ED Fig. 1d). Expression data (qPCR and flow cytometry) are compared with an unpaired student *t*-test (2 samples) or a one-way ANOVA with Tukey post-hoc test (more than 2 samples). Growth curves were fitted with a Gompertz model and the lag phases (*k* parameter) for each pair of *Lm* strains were compared with the extra sum-of-squares *F*-test (ED Fig. 2a). Half-lives were compared using the extra-sum of squares *F*-test (ED Fig. 6j). Proportion of cells with different colocalization patterns are compared with a contingency $\chi 2$ test (ED Fig. 1q and ED Fig. 7b, f). ns: $p>0.05$, *: $p<0.05$, **: $p<0.01$, ***: $p<0.001$, ****: $p<0.0001$.

Extended References

46. Shinkai, Y. *et al.* RAG-2-deficient mice lack mature lymphocytes owing to inability to initiate V(D)J rearrangement. *Cell* **68**, 855–867 (1992).
47. Malissen, M. *et al.* Altered T cell development in mice with a targeted mutation of the CD3-epsilon gene. *The EMBO journal* **14**, 4641–4653 (1995).
48. Kitamura, D., Roes, J., Kühn, R. & Rajewsky, K. A B cell-deficient mouse by targeted disruption of the membrane exon of the immunoglobulin mu chain gene. *Nature* **350**, 423–426 (1991).
49. Jung, S. *et al.* Analysis of fractalkine receptor CX(3)CR1 function by targeted deletion and green fluorescent protein reporter gene insertion. *Molecular and cellular biology* **20**, 4106–14 (2000).
50. Hameyer, D. *et al.* Toxicity of ligand-dependent Cre recombinases and generation of a conditional Cre deleter mouse allowing mosaic recombination in peripheral tissues. *Physiological genomics* **31**, 32–41 (2007).
51. Buch, T. *et al.* A Cre-inducible diphtheria toxin receptor mediates cell lineage ablation after toxin administration. *Nature methods* **2**, 419–426 (2005).
52. Matsuzawa, A. *et al.* A new allele of the lpr locus, lprcg, that complements the gld gene in induction of lymphadenopathy in the mouse. *The Journal of experimental medicine* **171**, 519–531 (1990).
53. Kägi, D. *et al.* Cytotoxicity mediated by T cells and natural killer cells is greatly impaired in perforin-deficient mice. *Nature* **369**, 31–37 (1994).
54. Huang, Q. Q. *et al.* FLIP: A novel regulator of macrophage differentiation and granulocyte homeostasis. *Blood* **116**, 4968–4977 (2010).
55. Huh, C.-G. *et al.* Hepatocyte growth factor/c-met signaling pathway is required for efficient liver regeneration and repair. *Proceedings of the National Academy of Sciences of the United States of America* **101**, 4477–4482 (2004).
56. Canli, Ö. *et al.* Myeloid Cell-Derived Reactive Oxygen Species Induce Epithelial Mutagenesis. *Cancer cell* **32**, 869-883.e5 (2017).
57. Monk, I. R., Gahan, C. G. M. & Hill, C. Tools for functional postgenomic analysis of listeria monocytogenes. *Applied and environmental microbiology* **74**, 3921–3934 (2008).
58. Arnaud, M., Chastanet, A. & Débarbouillé, M. New vector for efficient allelic replacement in naturally nontransformable, low-GC-content, gram-positive bacteria. *Applied and environmental microbiology* **70**, 6887–6891 (2004).
59. Argov, T., Rabinovich, L., Sigal, N. & Herskovits, A. A. An Effective Counterselection System for Listeria monocytogenes and Its Use To Characterize the Monocin Genomic Region of Strain 10403S. *Applied and environmental microbiology* **83**, (2017).
60. Balestrino, D. *et al.* Single-cell techniques using chromosomally tagged fluorescent bacteria to study Listeria monocytogenes infection processes. *Applied and Environmental Microbiology* **76**, 3625–3636 (2010).
61. Quereda, J. J. *et al.* A dual microscopy-based assay to assess Listeria monocytogenes cellular entry and vacuolar escape. *Applied and Environmental Microbiology* **82**, 211–217 (2016).
62. Disson, O. *et al.* Modeling human listeriosis in natural and genetically engineered animals. *Nature Protocols* **4**, 799–810 (2009).
63. Lu, H. *et al.* Subcutaneous Angiotensin II Infusion using Osmotic Pumps Induces Aortic Aneurysms in Mice. *Journal of Visualized Experiments* **2015**, (2015).

Acknowledgments: We thank Philippe Bousso and Alain Fischer for helpful discussions and the members of the Biology of Infection Unit for their support, in particular Laetitia Travier for technical help on brain microscopy and Lukas Hafner for contributing to data analysis. We thank the Cytometry and Biomarkers Unit of Technology and Service (CB UTechS), Dmity Ershov and Jean-Yves Tinevez from the Image Analysis Hub and the Center for Animal Resources and Research (C2RA) at Institut Pasteur. We are grateful to Geneviève de Saint Basile and Fernando Sepuvelda (Institut Imagine, Paris) for the Prf1 KO mice, Frédéric Rieux-Laucat (Institut Imagine, Paris) for the Fas^{lpr-cg} mice, Richard Pope for the $FLIP^{flox/flox}$ mice, Florian Greten for the $LysMCreER^{T2}$ mice, Alain Eychene for the $Met^{flox/flox}$ mice, and Javier Pizarro-Cerda and Pascale Cossart (Institut Pasteur) for the pAD β-lactamase plasmid. **Funding:** Work in ML laboratory is funded by Institut Pasteur, Inserm, ERC, ANR, DIM1HEALTH, Labex IBEID (ANR-10-LABX-62-IBEID) and Fondation Le Roch-Les Mousquetaires. CM and MK were recipient of the Roux-Cantarini fellowship of Institut Pasteur. LH, CG and JG were supported by Université de Paris, YHT by the Pasteur - Paris University (PPU) International PhD Program under the European Union's Horizon 2020 research and innovation program, Marie Sklodowska-Curie grant agreement No 665807, and SL by FRM (ECO201906009119) and “Ecole Doctorale FIRE-Programme Bettencourt”. ML is a member of Institut Universitaire de France.

Author contributions: ML initiated and coordinated the study. CM, MK, SL and ML conceived and designed the experimental strategy. CM & MK performed *in vivo* and cell sorting for *ex vivo* experiments. CM performed flow cytometry experiments. SL & YHT performed *in vivo* experiments and imaging of CNS tissue samples. JG performed *in vivo* experiments and imaging of infected intestinal tissue. OD & MK did *ex vivo* monocytes imaging. CM, LH and CG designed and performed RT-qPCR experiments. CM & LH performed cloning and

mutagenesis. MK performed western blotting experiments. CM, MK, SL, JG, OD, YHT and ML analyzed the data. CM, SL and ML wrote the manuscript, MK and OD edited it, and all authors agreed on its final version.

Competing interests: The authors declare no competing interests.

Data and material availability: The datasets generated and/or analyzed during the current study are available as Source Data.

Figure 1

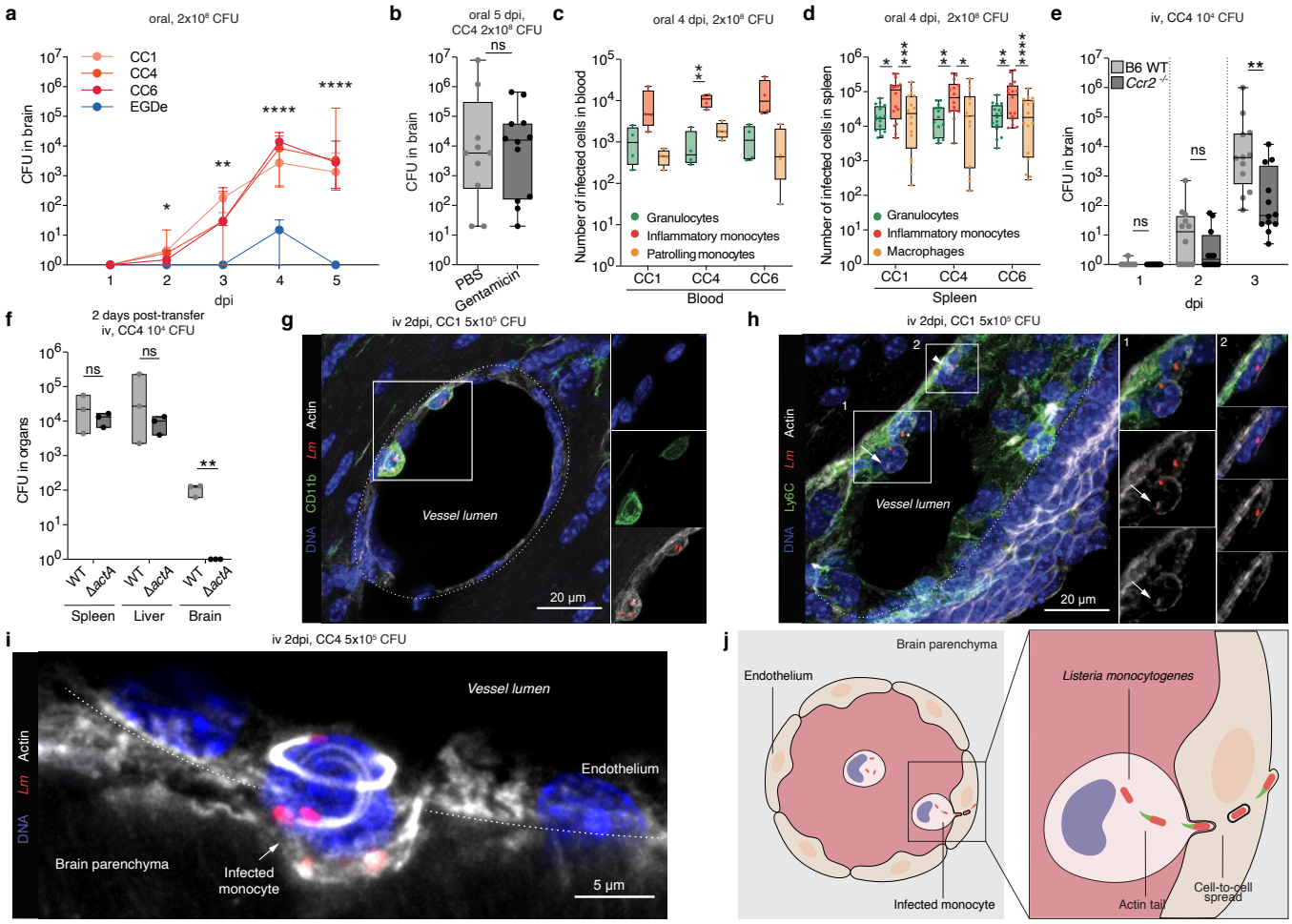
a
oral, 2x10⁸ CFU
CC1
CC4
CC6
EGDe
CFU in brain
dpi
b
oral 5 dpi, CC4 2x10⁸ CFU
ns
CFU in brain
PBS
Gentamicin
c
oral 4 dpi, 2x10⁸ CFU
Number of infected cells in blood
Granulocytes
Inflammatory monocytes
Patrolling monocytes
CC1
CC4
CC6
Blood
d
oral 4 dpi, 2x10⁸ CFU
Number of infected cells in spleen
Granulocytes
Inflammatory monocytes
Macrophages
Spleen
e
iv, CC4 10⁴ CFU
B6 WT
Ccr2 -/-
ns
CFU in brain
dpi
f
2 days post-transfer iv, CC4 10⁴ CFU
CFU in organs
WT
ΔactA
Spleen
Liver
Brain
g
iv 2dpi, CC1 5x10⁵ CFU
Actin
Lm
CD11b
DNA
Vessel lumen
20 µm
h
iv 2dpi, CC1 5x10⁵ CFU
Actin
Lm
Ly6C
DNA
Vessel lumen
20 µm
i
iv 2dpi, CC4 5x10⁵ CFU
Actin
Lm
DNA
Vessel lumen
Endothelium
Brain parenchyma
Infected monocyte
5 µm
j
Brain parenchyma
Endothelium
Infected monocyte
Listeria monocytogenes
Actin tail
Cell-to-cell spread

Figure 2

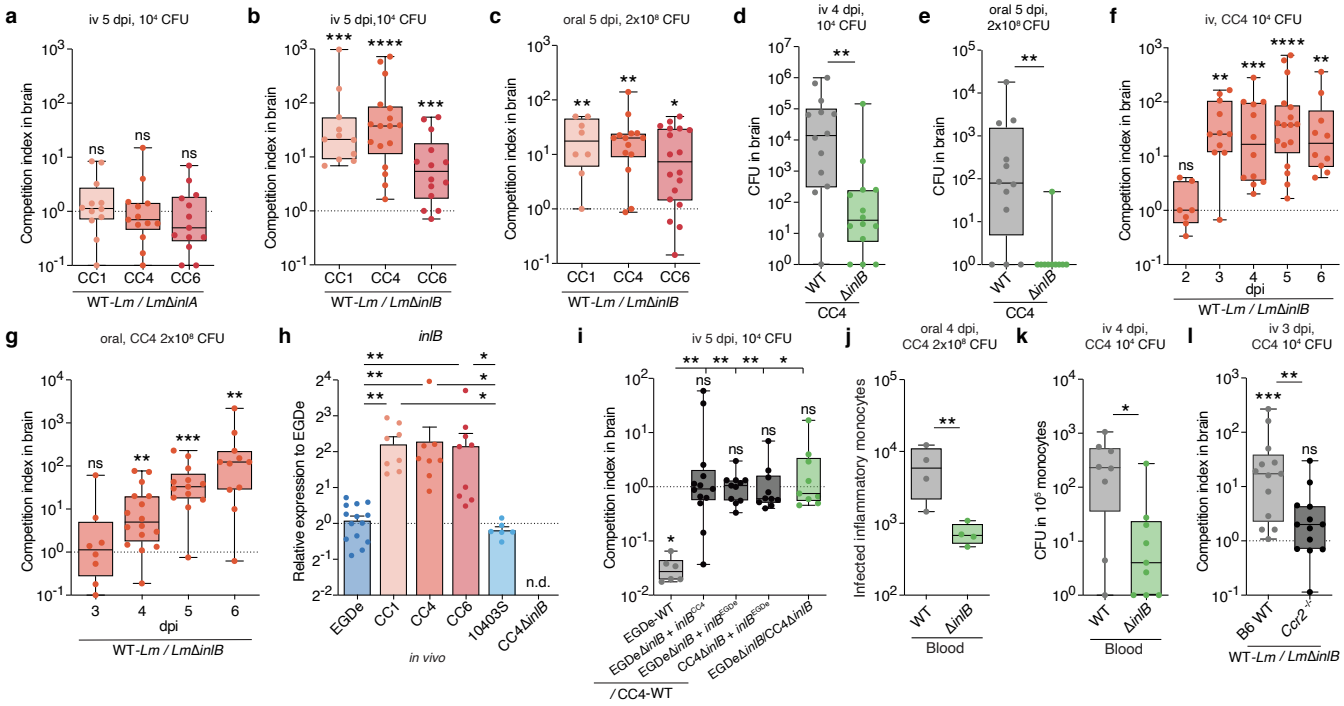
a
iv 5 dpi, 10⁴ CFU
Competition index in brain
CC1
CC4
CC6
WT-Lm / LmΔinlA
b
iv 5 dpi,10⁴ CFU
WT-Lm / LmΔinlB
c
oral 5 dpi, 2x10⁸ CFU
WT-Lm / LmΔinlB
d
iv 4 dpi, 10⁴ CFU
CFU in brain
WT
ΔinlB
CC4
e
oral 5 dpi, 2x10⁸ CFU
f
iv, CC4 10⁴ CFU
dpi
WT-Lm / LmΔinlB
g
oral, CC4 2x10⁸ CFU
h
inlB
Relative expression to EGDe
EGDe
10403S
CC4ΔinlB
n.d.
in vivo
i
iv 5 dpi, 10⁴ CFU
EGDe-WT
EGDeΔinlB + inlB^CC4
EGDeΔinlB + inlB^EGDe
CC4ΔinlB + inlB^EGDe
EGDeΔinlBCC4ΔinlB
/ CC4-WT
j
oral 4 dpi, CC4 2x10⁸ CFU
Infected inflammatory monocytes
Blood
k
iv 4 dpi, CC4 10⁴ CFU
CFU in 10⁵ monocytes
l
iv 3 dpi, CC4 10⁴ CFU
B6 WT
Ccr2-/-

Figure 3

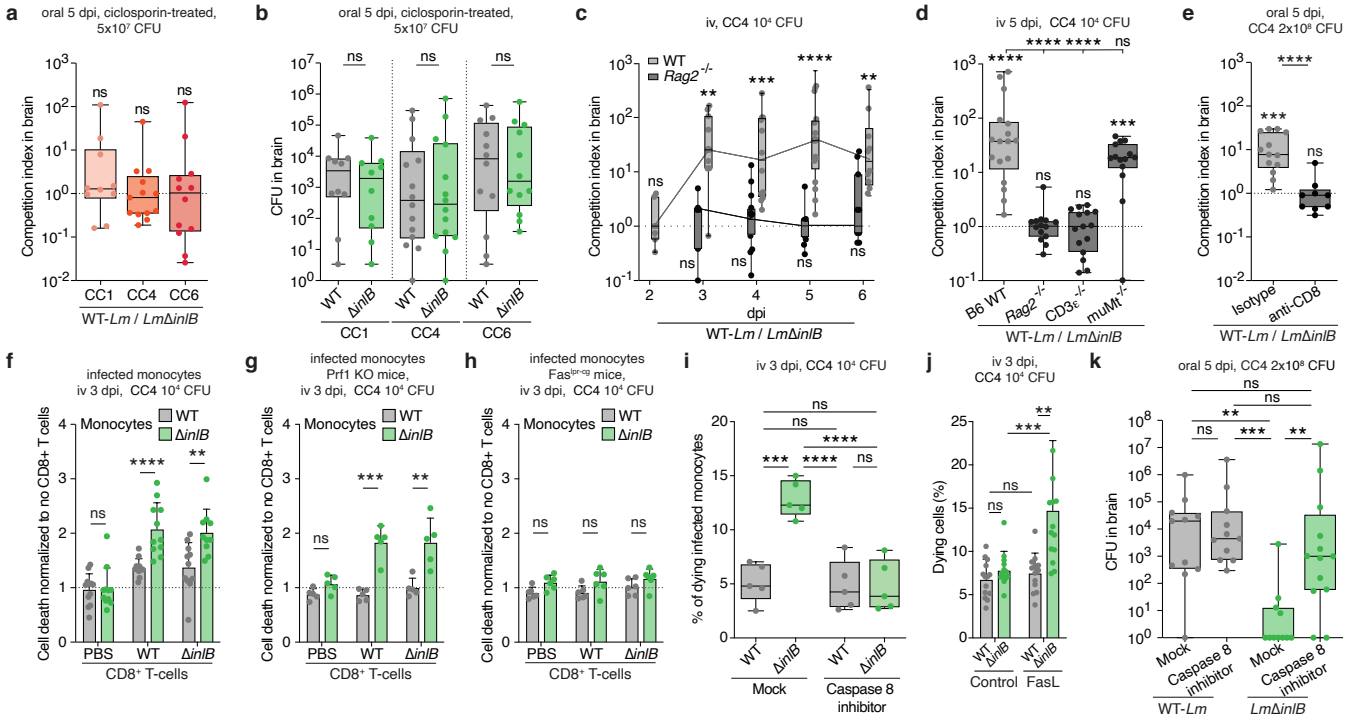
a
oral 5 dpi, ciclosporin-treated, 5x10⁷ CFU
Competition index in brain
CC1
CC4
CC6
WT-Lm / LmΔinlB
b
oral 5 dpi, ciclosporin-treated, 5x10⁷ CFU
CFU in brain
WT
ΔinlB
c
iv, CC4 10⁴ CFU
WT
Rag2 -/-
dpi
d
iv 5 dpi, CC4 10⁴ CFU
B6 WT
Rag2 -/-
CD3ε -/-
muMt -/-
e
oral 5 dpi, CC4 2x10⁸ CFU
Isotype
anti-CD8
f
infected monocytes
iv 3 dpi, CC4 10⁴ CFU
Monocytes
Cell death normalized to no CD8+ T cells
PBS
CD8+ T-cells
g
infected monocytes
Prf1 KO mice,
iv 3 dpi, CC4 10⁴ CFU
h
infected monocytes
Fasᵇʳ⁻ᶜᵍ mice,
iv 3 dpi, CC4 10⁴ CFU
i
iv 3 dpi, CC4 10⁴ CFU
% of dying infected monocytes
Mock
Caspase 8 inhibitor
j
iv 3 dpi, CC4 10⁴ CFU
Dying cells (%)
Control
FasL
k
oral 5 dpi, CC4 2x10⁸ CFU
Mock
Caspase 8 inhibitor
WT-Lm
LmΔinlB

Figure 4

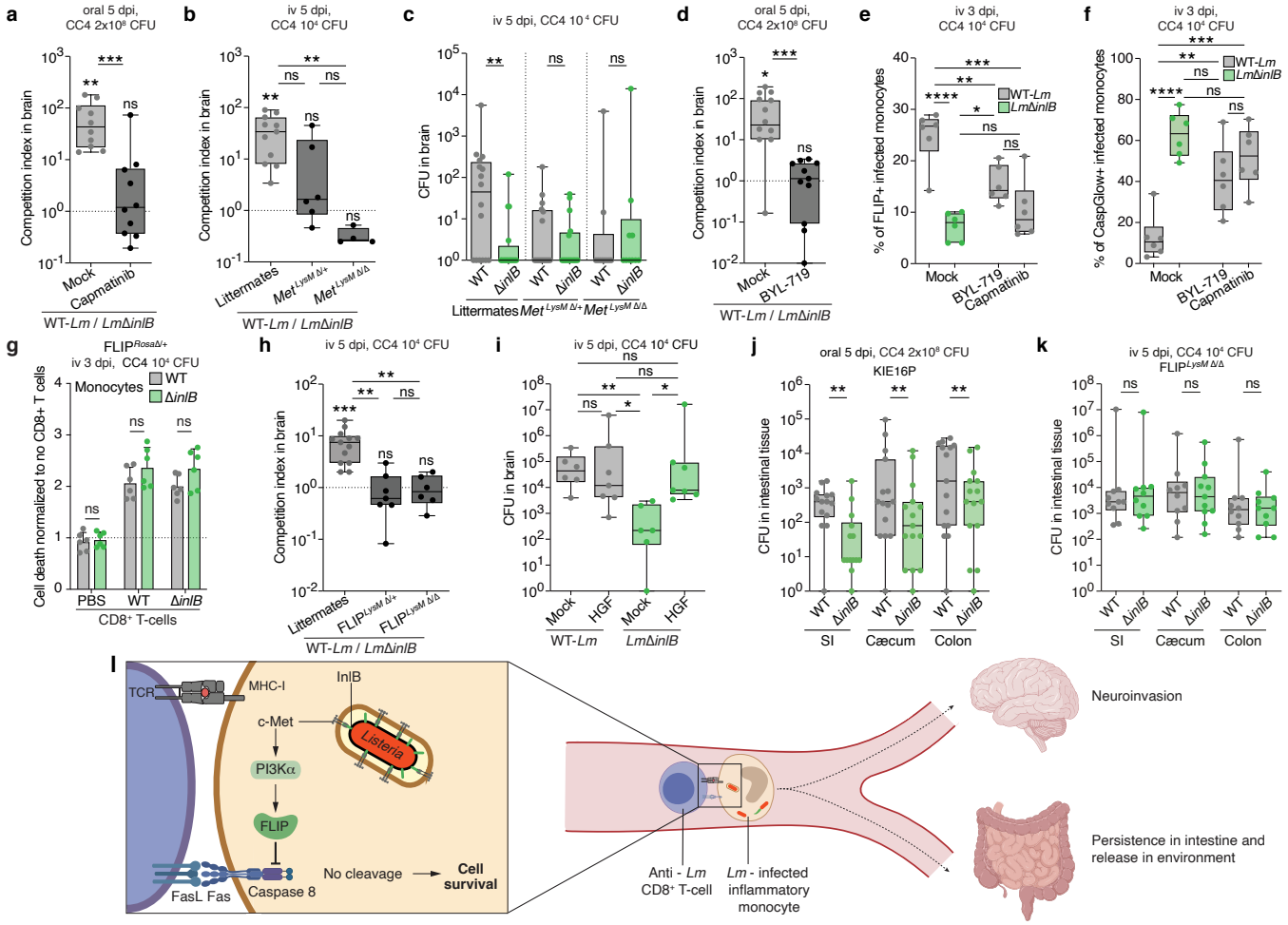
a
oral 5 dpi, CC4 2x10⁸ CFU
Competition index in brain
Mock
Capmatinib
WT-Lm / LmΔinlB
b
iv 5 dpi, CC4 10⁴ CFU
Competition index in brain
Littermates
Met LysM Δ/+
Met LysM Δ/Δ
WT-Lm / LmΔinlB
c
iv 5 dpi, CC4 10⁴ CFU
CFU in brain
WT
ΔinlB
Littermates
Met LysM Δ/+
Met LysM Δ/Δ
d
oral 5 dpi, CC4 2x10⁹ CFU
Competition index in brain
Mock
BYL-719
WT-Lm / LmΔinlB
e
iv 3 dpi, CC4 10⁴ CFU
% of FLIP+ infected monocytes
WT-Lm
LmΔinlB
Mock
BYL-719
Capmatinib
f
iv 3 dpi, CC4 10⁴ CFU
% of CaspGlow+ infected monocytes
WT-Lm
LmΔinlB
Mock
BYL-719
Capmatinib
g
FLIP RosaΔ/+
iv 3 dpi, CC4 10⁴ CFU
Cell death normalized to no CD8+ T cells
Monocytes
WT
ΔinlB
PBS
WT
ΔinlB
CD8⁺ T-cells
h
iv 5 dpi, CC4 10⁴ CFU
Competition index in brain
Littermates
FLIP LysM Δ/+
FLIP LysM Δ/Δ
WT-Lm / LmΔinlB
i
iv 5 dpi, CC4 10⁴ CFU
CFU in brain
Mock
HGF
WT-Lm
LmΔinlB
j
oral 5 dpi, CC4 2x10⁸ CFU
KIE16P
CFU in intestinal tissue
WT
ΔinlB
SI
Cæcum
Colon
k
iv 5 dpi, CC4 10⁴ CFU
FLIP LysM Δ/Δ
CFU in intestinal tissue
WT
ΔinlB
SI
Cæcum
Colon
l
TCR
MHC-I
InlB
c-Met
Listeria
PI3Kα
FLIP
FasL Fas
Caspase 8
No cleavage
Cell survival
Anti - Lm CD8⁺ T-cell
Lm - infected inflammatory monocyte
Neuroinvasion
Persistence in intestine and release in environment